A Structural Perspective on Prussian Blue Analogues for Aqueous Zinc-Ion Batteries
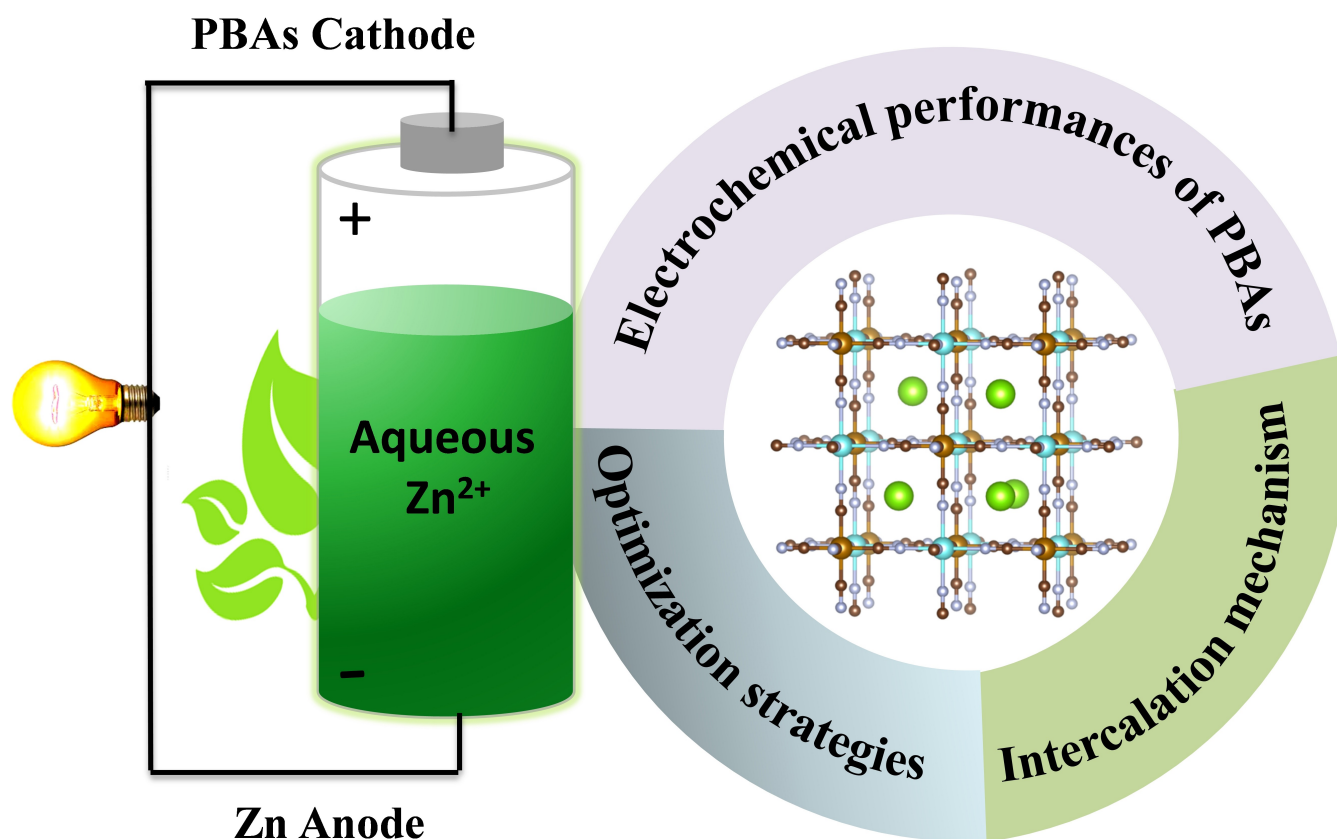
Min Li,[a] Mariam Maisuradze,[a] Rosalinda Sciacca,[a] Ivana Hasa,[b] and Marco Giorgetti*[a]

Aqueous zinc-ion batteries (AZIBs), have been identified as one of the most promising aqueous rechargeable metal-ion batteries (ARMIBs) for grid scale electrochemical energy storage application, and as such have received much attention by virtue of their unique properties including the high abundance of metallic zinc resources, their intrinsic safety, and cost effectiveness. Among the cathode materials used in AZIBs, Prussian Blue Analogues (PBAs) represent the most promising active materials in view of their improved cyclability and rate performance. Here, we provide a comprehensive review on recent progress on AZIBs obtained using PBAs cathodes with a particular focus on the present understanding of the structure-property correlation of different PBAs, which in turn guides further developments of improved cathode materials and optimization strategies to ensure an extended cyclability and capacity retention.

1. Introduction

Aqueous rechargeable metal-ion batteries (ARMIBs) are a promising class of batteries for grid-scale electrochemical energy storage due to their low-cost, high operational safety, and sustainability. Among the different systems proposed, sodium-ion, potassium-ion, magnesium-ion, calcium-ion, and zinc-ion batteries have been intensively discussed, owing to the abundancy and availability of the materials employed, high safety and environmental benignity.[1–5] Furthermore, aqueous electrolytes provide high ionic conductivity over non-aqueous systems, and the battery assembly process does not require controlled atmosphere, which simplifies the manufacturing process and lowers the associated costs.

Among the different ARMIBs, aqueous zinc-ion batteries (AZIBs) have attracted large attention for grid energy storage application, owing to the inherent advantages of Zn metal electrode and aqueous electrolyte.[4,6,7] Figure 1(a) summarizes theoretical gravimetric and volumetric capacity of different ARMIBs and the cost of the associated metals, highlighting the advantages of AZIBs compared to other systems. Historically, Zn electrodes had been used in the Volta pile, the first non-rechargeable battery, as early as in 1799. Later on, zinc has been widely used as anode for primary Leclanche cells {Zn (s)|ZnCl₂ (aq), NH₄Cl(aq)|MnO₂ (s) C(s)} and zinc chloride cells {Zn(s)|ZnCl₂(aq)|MnO₂(s)C(s)}, as well as second zinc-manganese dioxide cells {Zn(s)|KOH(aq)|MnO₂ (s)C(s)} and zinc-nickel oxide cells {Zn(s)|KOH(aq)|NiO(OH)(s)}, due to its low cost, nontoxicity, high theoretical gravimetric (820 mAh g⁻¹) and volumetric capacity (5855 mAh cm⁻³), and low standard reduction potential (−0.76 V vs. SHE).[6,8] In 1986, Shoji and coworkers first introduced the Zn|ZnSO₄(aq)|MnO₂ aqueous battery system, replacing the alkaline electrolyte with a zinc sulfate-based electrolyte, which overcame the drawbacks of alkaline

batteries in terms of cycling stability, and paved way to the study of aqueous neutral or weak acidic electrolytes for zinc-ion batteries.[9,10]

To date, the development of cathode materials for AZIBs mainly focused on manganese- and vanadium oxides, Prussian Blue Analogues (PBAs), organic and polyanion compounds,[11,12] as well as conversion type halogens.[13–15] Manganese-based materials, especially MnO_2, which has been used in primary and secondary batteries for years, are a very attracting class of materials because of their low cost, environmental-friendliness, and high theoretical capacity (~617 mAh g⁻¹ with Mn^{4+}/Mn^{2+} redox couple for 1 mol Zn^{2+} storage).[12,16] The basic local structure of MnO_2 is an octahedral unit composed of six oxygen atoms and one manganese atom. Depending on the number and connection of MnO_6 units, MnO_2 exhibits different crystal structures, including α-, β-, γ-, δ-, λ-, and r-types.[11] However, the low conductivity and the high dissolution of MnO_2 in aqueous electrolytes leads to significant capacity fading upon cycling, and poor rate performance, as well as a significant structure transformation affecting cell performance.[16–19] Different from the typical MnO_6 units in MnO_2, V−O coordination can change based on the V oxidation states, including tetrahedral, trigonal bipyramid, square pyramid, and distorted/regular octahedral.[20,21] The theoretical capacity of V_2O_5 is 294 mAh g⁻¹ based on V^{5+}/V^{3+} redox couple for 1 mol Zn^{2+} storage.[22,23] However, vanadium-based compounds present similar challenges as Mn-based materials, exhibiting unsatisfactory cycling performance. In addition, V-based electrode materials exhibit relatively low working potential, which leads to lower energy densities.[24,25]

Prussian blue analogues (PBAs), also known as metal hexacyanometallates, have attracted wide attentions as promising cathode material for ARZIBs. Generally, PBAs present a face center cubic structure, large ionic channels, and interstitial sites in the lattice. The physical and chemical properties of PBAs strongly depend on the different metals bonded to −CN- ligand. When the two metals are electroactive sites, the theoretical specific capacity of the PBAs can reach about 170 mAh g⁻¹ (considering 1 mol Zn^{2+} participate in the reaction), approaching values exhibited by well-known Li-ion battery cathode material including $LiMn_2O_4$ (148 mAh g⁻¹) and $LiFePO_4$ (170 mAh g⁻¹). Recently, PBAs have attracted large attention for implementation in the next generation sustainable battery chemistry such as sodium-ion batteries (SIBs).[26–28] Indeed, work conducted by Contemporary Amperex Technology Co. Limited (CATL) and Atris AB on the industrial development of SIBs have

[a] Dr. M. Li, M. Maisuradze, Dr. R. Sciacca, Prof. Dr. M. Giorgetti
Department of Industrial Chemistry "Toso Montanari"
University of Bologna
Viale Risorgimento 4, 40136 Bologna (Italy)
E-mail: marco.giorgetti@unibo.it
Homepage: http://www.unibo.it/sitoweb/marco.giorgetti/cv-en

[b] Prof. Dr. I. Hasa
Warwick Manufacturing Group (WMG)
University of Warwick
Coventry, CV4 7AL (United Kingdom)

Batteries & Supercaps

Review
doi.org/10.1002/batt.202300340

Chemistry
Europe

European Chemical
Societies Publishing

further demonstrated and confirmed the potential commercial application of these materials.

In this work, we review the electrochemical performance of different PBAs used as cathode materials in AZIBs. An overview of the structural properties of these materials and their modification following the reaction mechanisms in AZIBs is discussed. In particular, not only insertion/release of the Zn^{2+} ion has been proposed but also dramatic crystalline phase changes and proton intercalation have been observed so far. Furthermore, strategies to improve the electrochemical performances of PBAs are discussed. Finally, a summary of the challenges and outlook on the future research are given.

2. The structures of PB and PBAs

Prussian blue (PB), with the generic formula $A_xFe[Fe(CN)_6]$ (with A = alkali metal), has been known for more than 300 years since its discovery in 1710 (Figure 2).

During the 18th and 19th centuries, PB was wildly used as paint pigment and dye for coloring textiles.[27,29] The investigation of the structural properties of PB and the related compounds has been reported by Keggin and Miles, using X-ray analysis in 1936. Their studies demonstrated that PB has a cubic structure, with the ferrous and ferric iron atoms alternatively arranged at the corner of a cubic lattice, with the CN group lying on the edge. Alkali atoms are at the centers of alternate small cubes. In addition, their study proposed that for its reduced and oxidized form, i.e., the Prussian White (PW) and Berlin Green (BG), the same iron-cyanide skeleton structure remains, except for very slight changes in the Fe—Fe distances. Based on the Keggin-Miles structure, Ludi and co-workers presented the single crystal structure of PB in 1977.[31] They proposed a modified model that did not contain any uncoordinated interstitial transition-metal ions. The results showed that $Fe_4[Fe(CN)_6]_3 \cdot xH_2O$ exhibited a cubic primitive elementary cell (Pm3 m), which deviated from the well-known cubic (Fm3 m) phase, due to the presence of partly occupied vacancies. The distinction of the crystal structure of PB is related to the well-known "soluble" and "insoluble" forms. The "soluble" forms have a tendency to form colloidal solutions. Generally, the "soluble" forms contain alkali metals in the crystal lattice and present a typical face-centered cubic structure (F-43 m). The structure of the "insoluble" form also features a rigid cubic framework (Pm-3 m), without alkali metal, except that 1/4 of the $Fe(CN)_6^{4-}$ units are vacant, with the empty positions filled
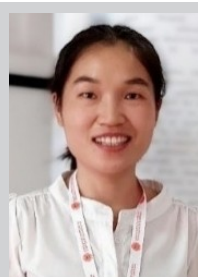
Min Li received her PhD in Analytical Chemistry, Department of Industrial Chemistry "Toso Montanari", University of Bologna in 2023. Her PhD study focuses on the synthesis and characterization of Prussian blue analogues for post-lithium-ion batteries. Currently, she is carrying post-doc job in University of Bologna with Prof. Dr. Marco Giorgetti, dedicating on synchrotron X-ray techniques and Operando and ex-situ analysis of high-performance energy storage systems.

Mariam Maisuradze is a PhD student at the Department of Industrial Chemistry at the University of Bologna. She has a chemistry background and is currently working on spectroscopical and electrochemical characterizations of the battery applications. Her research topic mainly concerns the hexacyanoferrate compounds as potential cathode materials, especially in post-lithium, aqueous systems, and the investigation of their working mechanism, as well as the structural properties, by employing mostly X-ray characterization techniques.

Rosalinda Sciacca is currently a post-doctoral researcher at the Department of Industrial Chemistry of the University of Bologna. Her research mainly deals with the synthesis, characterization and electrochemical performances of Prussian Blue Analogues as ion-exchangers both in the environmental and the energy fields. In addition, her PhD thesis also focused on the corrosion process of metallic artefacts for the cultural heritage protection. She is specialized in the electrochemical and analytical techniques.

Ivana Hasa is an Assistant Professor of Electrochemical Materials at the University of Warwick (WMG). She is a chemist by background with extensive experience on electrochemical energy storage systems. Her research activities are directed toward the understanding of the processes governing the chemistry of the next generation sustainable battery technologies. Design of technically relevant materials and the investigation of their structure-property correlation and electrochemical behavior are the core of her research interest. Her work is inherently interdisciplinary, tackling challenges at the interface of chemistry, materials science, electrochemistry, and the scale up of new battery chemistries to full proven cell prototypes.

Marco Giorgetti is an Associate Professor of Analytical Chemistry, and he leads the group of Spectroscopy Electrochemistry and Energy (S2 C) at the University of Bologna. His research interest covers the field of the structural and electronic characterization of materials and solutions by core level spectroscopies, such as X-ray Spectroscopies, the applied electrochemistry, sensors, the synthesis and characterization of materials for advanced batteries. He has applied Prussian blue-based materials in potentiometric and amperometric sensors, ion exchange, batteries. He is an expert in methodologies for data analysis. He had pioneered the in-situ characterization of energy material by the x-ray absorption synchrotron radiation technique.
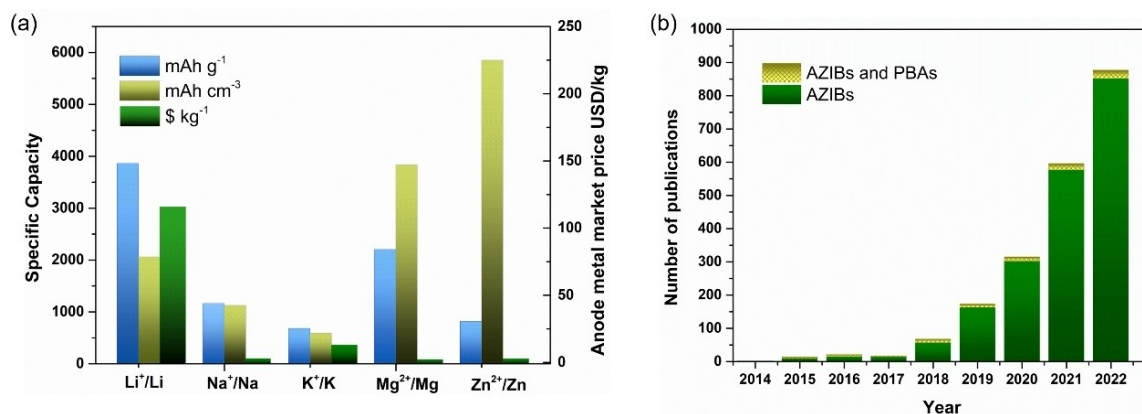
Batteries & Supercaps

Review

doi.org/10.1002/batt.202300340

Chemistry Europe
European Chemical
Societies Publishing

Figure 1. a) Theoretical gravimetric/volumetric capacity and anode metal market price of Li/Na/K/Mg/Zn metals (metal price were taken from "price.metal.com. Shanghai Metals Market. 2020-02-03"). b) Number of scientific peer-reviewed publications on AZIBs, as well as PBAs and AZIBs (data collected in June 2023 from Clarivate web of science. Keywords used "Aqueous Zinc-ion Battery", and "Aqueous Zinc-ion Battery" &" Hexacyanoferrate or Prussian blue analogues").
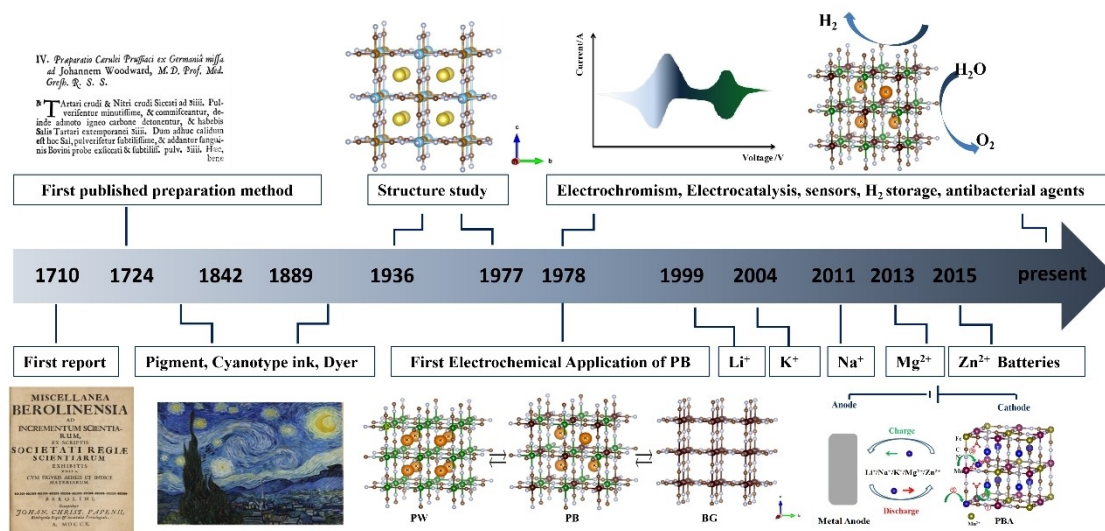

Figure 2. Timeline of study and application of PBAs.

out by water molecules in order to complete the coordination shell of M′ sites (Figure 3a, b).[31–33] As these water molecules are structurally coordinated by the metal sites, they are usually referred to as "structural" and affect the electrode performance in batteries dramatically.[34–38]

When Fe-sites in PB are substituted by other transition metals, a class of hexacyanometallates, generally called Prussian Blue Analogues (PBAs) can be derived with general formula $A_xM[M'(CN)_6]_{1-y}\square_y \cdot zH_2O$ ($0 \leq x \leq 2$, $0 < y < 1$), where A is alkali-metal ion, M and M′ are transition metal ions, $\square$ represents the $M'(CN)_6$ vacancies, and the H_2O includes both interstitial and coordination water. Generally, the most studied PBAs are metal hexacyanoferrates, with the Fe being coordinated by the carbon side of the cyanide group. Since V. D. Neff[39] reported about the electrochemical activity of PB in 1978, PB and PBAs have been widely studied for their electrochromic properties,[40–42] in electrocatalysis,[30,43] for potentiometric and amperometric sensors,[44,45] and lately, as electrode materials in electrochemical energy storage systems.[46–50] Generally, in hexacyanoferrates,

the involved transition metals (M) and Fe are octahedrally coordinated with N atoms and C atoms of −CN- ligands within a cubic unit cell, resulting in a well-defined high-spin ($M^{HS}N_6$) and low spin state ($Fe^{LS}C_6$) because of the weak N-coordinated and strong C-coordinated crystal fields. The diversity in chemical composition and large interstitial sites (> 3.5 Å) able to accommodate a large number of $A^{+/2+/3+}$ ions, enable PBAs to present different structures and associated electrochemical properties.[28,51]

3. PBAs as Cathode Materials for AZIBs Application

Benefitting from their 3D opened framework and large ion channels, PBAs are excellent intercalation materials for battery applications, and as such have been widely used as electrode material for both Li-ion batteries and post-Li-ion batteries.[46,52–57]

Batteries & Supercaps

Review
doi.org/10.1002/batt.202300340

Chemistry Europe
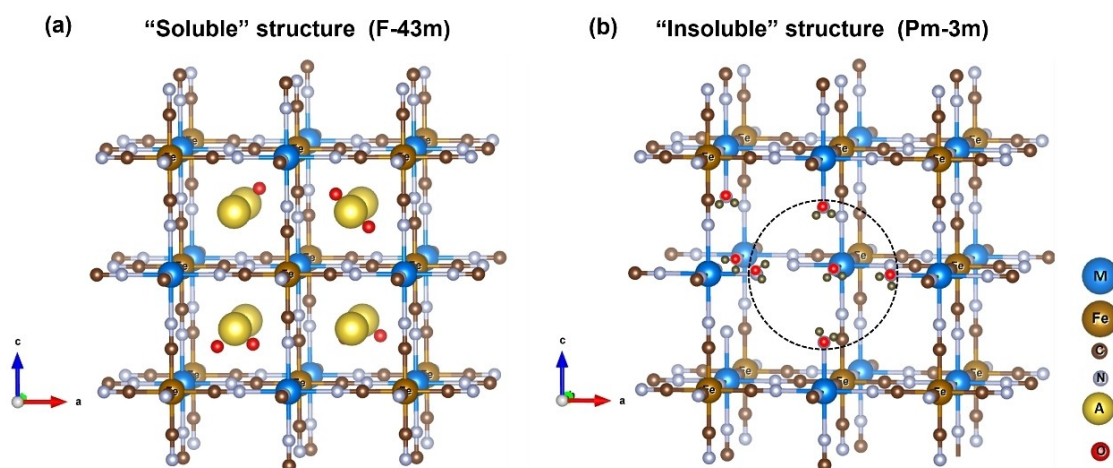European Chemical
Societies Publishing

Figure 3. Unit cell of a) soluble and b) insoluble structure of $A_xM[Fe(CN)_6]_{1-y}\square_y \cdot zH_2O$

The implementation of PBAs in AZIBs was first reported by Jia et al.[58] in 2015, demonstrating reversible insertion of Zn^{2+} ions in copper hexacyanoferrate (CuHCF) nano-cubes when employing aqueous electrolyte. Following the initial studies, different PBAs were studied as a cathode material for AZIBs, including zinc hexacynoferrate (ZnHCF), nickel hexacynoferrate (NiHCF), PB, manganese hexacynoferrate (MnHCF), cobalt hexacynoferrate (CoHCF), and vanadium hexacynoferrate (VHCF). Table 1 schematically summarizes the electrochemical performance of different PBAs in AZIBs proposed so far, for which several review papers are available.[59,60] Within this review further elaborate on the most recent progress adopting a structural perspective, in order to offer an account on the present understanding of the structure-activity relationship of these PBAs AZIBs systems, and the strategies for their optimization.

3.1. The study of PBAs reaction mechanism in AZIBs

It is widely accepted that the adopted reaction mechanism in PBAs-based AZIBs is the (de−)insertion of ions, however relevant structural changes occurring upon cycling and their corresponding stability strongly affects their electrochemical response.

The structure of PBAs in aqueous Zn-ion electrolytes is very different when compared to Li-/Na-/K -ion organic-based electrolytes, in which the basic hexacyanoferrate network of PBAs is stable upon the ion (de-)insertion. On the contrary, in aqueous Zn-ion electrolytes, the ion-insertion process seems to not only occur at the interstitial sites during discharge, but also happened at the lattice sites, especially at the N-connected metal sites for some PBAs. This unconventional reactivity was also observed for PB in cadmium containing electrolyte.[109,110]

Several different Zn^{2+} storage mechanisms have been proposed for the widely-used manganese-based oxide including Zn^{2+} insertion/extraction, H^+ and Zn^{2+} co-insertion, and chemical conversion.[16,18,19,111–117] Compared to this extensive research, the application and the investigation of the reaction

mechanism of PBAs in ARZIBs are quite limited (Figure 1b). In the following sections, the reaction mechanism for relevant PBAs, and their interplay with the electrochemical response in AZIBs is presented.

3.1.1. CuHCF

CuHCF with repeating —Cu—NC—Fe- units, exhibits a typical face-center cubic structure (Figure 4a). Due to its ultra-low strain open framework structure, an extremely long cycle life (40,000 cycles) and high-rate capability (83 C) was reported by Wessells et al.[54] in aqueous (1 M KNO_3/0.01 M HNO_3) electrolyte. The application of CuHCF in AZIBs was first demonstrated by Jia et al.,[58] using a three-electrode cell setup in aqueous $ZnSO_4$ (1 M) electrolyte. A maximum discharging capacity of 56 mAh g^{-1} was obtained at a current density of 20 mA g^{-1}, and 77% capacity retention was observed after 20 cycles. Another zinc-ion cell including a CuHCF cathode and a Zinc foil anode with a $ZnSO_4$ (20 mM) solution was reported by Trocoli et al. in the same year.[61] The average operating voltage of the cell was as high as 1.73 V, and the cell could provide 90% of the theoretical capacity with a capacity retention of 96.3% after 100 cycles when cycled at 1 C.

A series of studies on the use of CuHCF in aqueous Zinc-ion cells, including the investigation of the aging mechanism of CuHCF in different electrolytes, and the structural phase transformation upon cycling have been reported by La Mantia and coworkers.[59,62,63,118–121] By combing post-mortem X-ray diffraction and electron microscopy analysis, it was found that a new secondary phase based on Cu/Zn PB was formed during cycling (Figure 4b). The suggested mechanism included the formation of a cubic $Zn_3[Fe(CN)_6]_2$ phase, due to the substitution of Cu ions by Zn ions (Equation 1) followed by the formation of an intermediate compound containing both Zn and Cu ions (Equation 2) and a final substitution of Fe sites by Zn^{2+} and/or Cu^{2+} ions [Equation (3)].

Table 1. Electrochemical parameters derived from aqueous Zn-ion cells reported in literature.

Cell set-up for AZIBs Cathode | Anode | or (reference)	Electrolyte	Discharge plateau [V]	Specific capacity [mAh g⁻¹ @mAg⁻¹]	Capacity retention in [%], cycles @ [mAg⁻¹]	Ref.
CuHCF | graphite disk | SCE	1 M $ZnSO_4$	0.8–0.5 V vs. SCE	56 mAhg⁻¹@20 mAg⁻¹	77%, 20cycles @20 mAg⁻¹	[58]
$K_{0.71}$Cu[Fe(CN)$_6$]$_{0.72}$·3.7H$_2$O | Zn foil | Ag/AgCl	20 mM $ZnSO_4$	1.73 V vs. Zn^{2+}/Zn	60 mAhg⁻¹@1 C	96.3%, 100cycles @1 C	[61]
CuHCF | Zn foil | Ag/AgCl	0.1 M Zn(ClO$_4$)$_2$ + 2 M NaClO$_4$	1.0 V vs.NHE	~55 mAhg⁻¹	82%, 500 cycles	[62]
CuZnHCF (93:7) | Zn foil | Ag/AgCl	20 mM $ZnSO_4$	0.53 V vs. Ag/AgCl	449 W kg⁻¹ at 5 C	85.54%, 1000 cycles@ 1 C	[63]
$K_{2x/3}$Cu[Fe(CN)$_6$]$_{2/3}$·3.4H$_2$O | Zn metal	1 M $ZnSO_4$	1.6 V vs. Zn^{2+}/Zn	60 mAhg⁻¹@1 C	95.8%, 50 cycles @ 1 C	[64]
$K_{0.72}$Cu[Fe(CN)6]$_{0.78}$·3.7H$_2$O | Zn metal	1 M (NH$_4$)$_2$SO$_4$ and 0.1 M $ZnSO_4$	1.8 V vs. Zn^{2+}/Zn	70.4 mAhg⁻¹ @ 300 mAg⁻¹	76.5%, 1000 cycles @1800 mAg⁻¹	[65]
CuHCF | Zn foil	NaCl/$ZnSO_4$/sodium alginate	2.1 V vs. Zn^{2+}/Zn	260 mAhg⁻¹ @ 1 Ag⁻¹	96.8%, 450 cycles @1 Ag⁻¹	[66]
K_2Zn_3[Fe(CN)$_6$]$_2$(H$_2$O)$_9$ | Pt | SCE	1 M $ZnSO_4$	1.7 V vs. Zn^{2+}/Zn	73.7 mAhg⁻¹@1 C	76%, 100 cycles @0.5 C	[67]
ZnHCF@MnO$_2$ | Zn foil	$ZnSO_4$/poly(vinyl alcohol) (PVA) gel	1.7 V vs. Zn^{2+}/Zn	89 mAhg⁻¹ @ 100 mAg⁻¹	77%, 1000 cycles @ 500 mAg⁻¹	[68]
ZnHCF CNT sheets | Zn nanosheet arrays	$ZnSO_4$–CMC gel	> 1.8 V vs. Zn^{2+}/Zn	100.2 mAhcm⁻³ @ 0.1 Acm⁻³	91.8%, 200 cycles	[69]
$K_{0.02}$(H$_2$O)$_{0.22}$Zn$_{2.94}$[Fe(CN)$_6$]$_2$ | Zn$_2$Mo$_6$S$_8$	0.1 M Zn(SO$_4$)$_2$	1.75 V vs. Zn^{2+}/Zn	62.5 mAhg⁻¹ @ 0.5 C	81%, 10cycles @0.5 C	[70]
ZnHCF | Zn sheet	1 M (Zn(CF$_3$SO$_3$)$_2$) hierarchical polymer electrolyte	1.9/1.8 V vs. Zn^{2+}/Zn	67 mAhg⁻¹ @ 2.5 C	80%, 250 cycles @2.5 C	[71]
$K_{0.336}$Zn$_{2.486}$[Fe(CN)$_6$]$_2$·3.09H$_2$O | Zn	0.5 M $ZnSO_4$/0.05 M K$_2$SO$_4$ hybrid electrolytes	1.937 V vs. Zn^{2+}/Zn	69.1 mAhg⁻¹ @ 2 C	86.4%, 100 cycles @10 C	[72]
MnZnHCFs | Zn foil	1 M $ZnSO_4$	1.75 V vs. Zn^{2+}/Zn	41.6 mAhg⁻¹ @ 50 mAg⁻¹	94%, 500 cycles at 250 mAg⁻¹	[73]
ZnHCF | PANI	7.5 M ZnCl$_2$ with 4 M NaCl additive	1.8/1.2 V vs. Zn^{2+}/Zn	150 mAhg⁻¹ @ 0.1 Ag⁻¹	75.2%, 300 cycles @0.5 Ag⁻¹	[74]
NiHCF | Zn	0.5 M Na$_2$SO$_4$ and 50 mM $ZnSO_4$	~1.6–1.4 V vs. Zn^{2+}/Zn	76.2 mAhg⁻¹ @ 100 mAg⁻¹	81%, 1000 cycles@ 500 mAg⁻¹	[75]
$K_{0.86}$Ni[Fe(CN)$_6$]$_{0.954}$(H$_2$O)$_{0.766}$ | Zn	0.5 M Zn(ClO$_4$)$_2$ acetonitrile	1.19 V vs. Zn^{2+}/Zn	55.6 mAhg⁻¹ @ 0.2 C	90%, 35 cycles @ 0.2 C	[76]
NiHCF | Zn	1 M Na$_2$SO$_4$ and 20 mM $ZnSO_4$	1.464 V vs. Zn^{2+}/Zn	74.1 mAhg⁻¹ @ 100 m Ag⁻¹	91%, 1000 cycles @ 500 mAg⁻¹	[77]
$K_{1.29}$Ni[Fe(CN)$_6$]$_{0.821}$·2.64H$_2$O | Zn	1 M Zn(TFSI)$_2$ + 21 M LiTFSI	~1.7~1.5 V vs. Zn^{2+}/Zn	67.9 mAhg⁻¹ @ 0.2 C	88.6%, 1600 cycles @ 0.5 C	[78]
NiHCF | RGO	2 M $ZnSO_4$	~1.58 V vs. Zn^{2+}/Zn	94.5 mAhg⁻¹ @ 5 mAg⁻¹	80.3%, 1000 cycles @ 200 mAg⁻¹	[79]
$K_{0.05}$Fe(III)[Fe(III)(CN)$_6$]·2.6H$_2$O | Zn wire	bio-ionic liquid-water electrolyte: 1.0 M Zn(OAc)$_2$/([Ch]OAc+30 wt % water)	~1.1 V vs. Zn^{2+}/Zn	120 mAhg⁻¹ @ 10 mAg⁻¹	95.8%, 10 cycles @ 10 mAg⁻¹	[80]
Na$_{0.61}$Fe$_{1.94}$(CN)$_6$□$_{0.06}$ | Zn foil	1 M Na$_2$SO$_4$	~1.1 V vs. Zn^{2+}/Zn	73.5 mAhg⁻¹ @ mAg⁻¹	80%, 1000 cycles @ 300 mAg⁻¹	[81]
FeHCF | Zn sheet	21 M LiTFSI and 1 M Zn(NTF$_2$)$_2$	~1.5 V vs. Zn^{2+}/Zn	78 mAhg⁻¹ @ 3 Ag⁻¹	73%, 10000 cycles @ 3 Ag⁻¹	[82]
Na$_{1.45}$Fe[Fe(CN)$_6$]$_{0.93}$·3.2H$_2$O | Zn	1 M (NH$_4$)$_2$SO$_4$ and 20 mM $ZnSO_4$	1.3 V vs. Zn^{2+}/Zn	73.6 mAhg⁻¹ @ 0.25 Ag⁻¹	92.1%, 2000 cycles @ 2 Ag⁻¹	[83]
Na$_{1.03}$Fe[Fe(CN)$_6$]$_{0.96}$·2H$_2$O | Zn	7 M NaCF$_3$SO$_3$/0.1 M Zn(CF$_3$SO$_3$)$_2$ + 2 vol% vinylene carbonate solution	1.1 V vs. Zn^{2+}/Zn	75 mAhg⁻¹ @ 1 C	60%, 4000 cycles @ 10 C	[84]
FeHCF | Zn plate	1 M Na$_2$SO$_4$ + 20 mM $ZnSO_4$	~1.0/0.2 V vs. SCE	141.6 mAhg⁻¹ @ 100 mAg⁻¹	77.5%, 800 cycles @ 1 Ag⁻¹	[85]
FeHCF | Pt | Ag/AgCl	1 M NaTfO and 0.1 M Zn(TfO)$_2$ ACN/H$_2$O	1.04 V vs. Ag/AgCl	69.1 mAhg⁻¹ @ 10 C	51.4%, 19000 cycles @ 10 C	[86]
FeHCF | Zn foil	3 M Zn(OTf)$_2$ + 3 M KOTf	1.7/1.0 V vs. Zn^{2+}/Zn	169.2 mAhg⁻¹ @ 100 mAg⁻¹	57%, 1000 cycles @ 1 Ag⁻¹	[87]
[Fe(CN)$_6$]$_{0.93}$□$_{0.07}$·1.54H$_2$O | Zn foil	1.5 M KCF$_3$SO$_3$ + 0.5 M Zn(CF$_3$SO$_3$)$_2$ in triethyl phosphate (TEP)/H$_2$O	1.85/1.15 V vs. Zn^{2+}/Zn	142 mAhg⁻¹ @ 0.1 Ag⁻¹	80.5%, 3000 cycles @ 1 Ag⁻¹	[88]
Na$_3$MnFe(CN)$_6$ | Zn sheet	1 M Na$_2$SO$_4$ and $ZnSO_4$+sodium dodecyl sulfate (SDS) aqueous electrolyte.	1.8/1.65/1.4 V vs. Zn^{2+}/Zn	137 mAhg⁻¹ @ 0.5 C	90%, 400 cycles @ 0.5 C	[89]

Table 1. continued

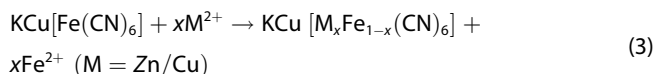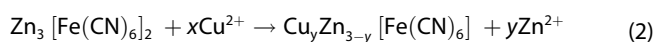| Cell set-up for AZIBs Cathode | Anode | or (reference)	Electrolyte	Discharge plateau [V]	Specific capacity [mAh g⁻¹ @mAg⁻¹]	Capacity retention in [%], cycles @ [mAg⁻¹]	Ref.
MnCoHCF (0.50) | graphite rod | Ag/AgCl	1 M Zn $(ClO_4)_2$	~0.8 V vs. Ag/AgCl	111 mAhg⁻¹ @ 25 mAg⁻¹	93%, 100 cycles @ 100 mAg⁻¹	[90]
$K_2MnFe (CN)_6$ | zinc metal	2 M Zn $(ClO_4)_2$ in tetraethylene glycol dimethyl ether	1.6 V vs. Zn^{2+}/Zn	65.5 mAhg⁻¹ @ 25 mAg⁻¹	94%, 8500 cycles @ 200 mAg⁻¹	[91]
CoMnPBA hollow sphere | zinc foil	2.0 M Zn $(CF_3SO_3)_2$	~1.5 V vs. Zn^{2+}/Zn	128.6 mAhg⁻¹ @ 0.05 A g⁻¹	76.4%, 1000 cycles @ 1 A g⁻¹	[92]
KMHCF-PVP-80 | metallic zinc	1 M $ZnSO_4$ + 0.1 M Mn SO_4	1.4/1.2 V vs. Zn^{2+}/Zn	140 mAhg⁻¹ @ 1 C	60.7%, 400 cycles @1C	[93]
NaMnHCF | Pt | Ag/AgCl	1 M $ZnSO_4$	0.8~0.9 V vs. Ag/AgCl	55.3 mAhg⁻¹ @ 50 mAg⁻¹	60%, 120 cycles @ 50 mAg⁻¹	[94]
$K_{1.6}Mn [Fe (CN)_6]_{0.94}·0.63H_2O$ | Zn foil	30 M KFSI + 1 M Zn $(CF_3SO_3)_2$	1.74 V vs. Zn^{2+}/Zn	138 mAhg⁻¹ @ 0.2 A g⁻¹	72.5%, 400 cycles @ 0.2 A g⁻¹	[95]
MnHCF | zinc metal	3 M $ZnSO_4$	1.78/1.42 V vs. Zn^{2+}/Zn	176 mAhg⁻¹ @ C/20	~70%, 50 cycles @ C/5	[96]
$K_{1.76}Mn_{1.17}[Fe (CN)_6]·xH_2O$ | Zn foil	3 M Zn $(OTf)_2$	~1.8–1.7 V and 1.3–1.1 V vs. Zn^{2+}/Zn	123 mAhg⁻¹ @ 50 mAg⁻¹	90%, 500 cycles @ 250 mAg⁻¹	[97]
CuMn–PBA double-shelled nanoboxes (DSNBs) | zinc foil	3 M LiTFSI + 2 M Zn $(CF_3SO_3)_2$	1.7–1.5 V vs. Zn^{2+}/Zn	116.8 mAhg⁻¹ @ 0.1 A g⁻¹	96.8%, 2000 cycles @ 1 A g⁻¹	[98]
MnHCF | MnO_2	2 M $ZnSO_4$ + 0.1 M $MnSO_4$	~1.4 V vs. Zn^{2+}/Zn	287 mAhg⁻¹ @ 0.1 A g⁻¹	87.1%, 70 cycles @ 0.1 A g⁻¹	[99]
MnO_2@MnHCF–PPy | Zn slice	$ZnSO_4$/poly (vinyl alcohol)	1.75 V vs. Zn^{2+}/Zn	263 mAhg⁻¹ @ 0.5 C	87%, 200 cycles @ 0.5 C	[100]
$Na_3MnFe (CN)_6$@PPy | Zn foil	1 M $NaCF_3SO_3$ + 1 M Zn $(CF_3SO_3)_2$	~1.4 V vs. Zn^{2+}/Zn	55 mAhg⁻¹ @ 200 mAg⁻¹	86.5%, 150 cycles @ 200 mAg⁻¹	[101]
$CoFe (CN)_6$ | Zn	4 M Zinc Trifluoromethanesulfonate (Zn $(OTf)_2$)	~1.75 V vs. Zn^{2+}/Zn	173.4 mAhg⁻¹ @ 0.3 A g⁻¹	100%, 2200 cycles @ 200 mAg⁻¹	[102]
CoHCF | Zn	2 M Zn $(BF_4)_2$ + ((EMIM)BF_4) ionic liquid	~1.7 V vs. Zn^{2+}/Zn	187.3 mAhg⁻¹ @ 0.25 A g⁻¹	98%, 40000 cycles @ 4 A g⁻¹	[103]
CC@Co-HCF@PEDOT: PSS | Pt | Ag/AgCl	2 M $ZnSO_4$	~0.8 V vs. Ag/AgCl	129.5 mAhg⁻¹ @ 0.1 A g⁻¹	95.5%, 1000 cycles @ 1 A g⁻¹	[104]
VHCF | Zn	4 M Zn $(CF_3SO_3)_2$	1.85/1.71, 1.12/0.92, 0.71/0.51 V vs. Zn^{2+}/Zn	187 mAhg⁻¹ @ 0.5 A g⁻¹	87.8%, 1000 cycles @ 2 A g⁻¹	[105]
VHCF | Zn	3 M Zn $(CF_3SO_3)_2$ + 10 M LiTFSI	~1.8 V vs. Zn^{2+}/Zn	235.8 mAhg⁻¹ @ 0.2 A g⁻¹	92.9%, 1000 cycles@ 5 A g⁻¹	[106]
VO–PBA | Zn	21 M LiTFSI and 1 M Zn $(CF_3SO_3)_2$	1.68/1.60, 1.05/0.95, 0.64/0.42 V vs. Zn^{2+}/Zn	209.6 mAhg⁻¹ @ 0.1 A g⁻¹	95.5%, 2000 cycles @ 1 A g⁻¹	[107]
VHCF/CNTs | Zn foil	2 M $ZnSO_4$	1.8–1.6 V vs. Zn^{2+}/Zn	97.8 mAhg⁻¹ @ 50 mAg⁻¹	52.7 mA h⁻¹ after 1000 cycles @ 3200 mAg⁻¹	[108]
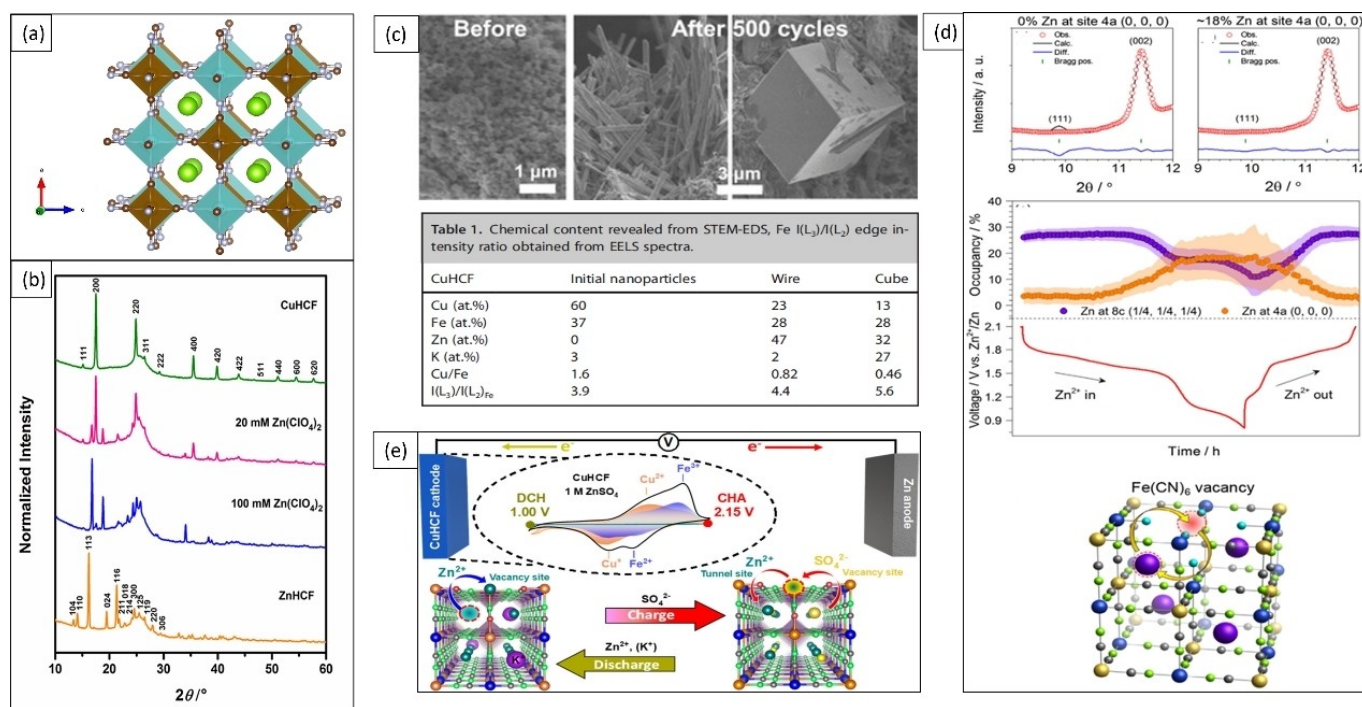
Figure 4. a) Structure model of CuHCF. b) XRD diffractograms of pristine CuHCF, ZnHCF, and CuHCF after 500 cycles in 20 and 100 mM $Zn(ClO_4)_2$ aqueous solutions. Reproduced with permission from Ref. [118] Copyright (2016) Elsevier Ltd. All rights reserved. c) SEM images and chemical content of wire and cube morphologies which form after 500 cycles in comparison to the initial CuHCF cathode surface. Reproduced with permission from Ref. [119] Copyright (2019) Wiley-VCH Verlag GmbH & Co. KGaA. d) Zn^{2+} swapping between the tunnel sites and Fe $(CN)_6$ sites. Reproduced with permission from Ref. [64]. Copyright (2017) The Authors. Published by Elsevier B.V. e) Schematic representation demonstrating that Zn^{2+}/SO_4^{2-} ions from the electrolyte partially intercalate into graphitic carbon domains and/or crystallize close to the surface regions. Reproduced with permission from Ref. [122]. Copyright (2021) The Authors. Published by American Chemical Society.

$$2KCu[Fe(CN)_6] + 3Zn^{2+} \rightarrow Zn_3[Fe(CN)_6]_2 + 2Cu^{2+} + 2\ K^+ \quad (1)$$

$$Zn_3[Fe(CN)_6]_2 + xCu^{2+} \rightarrow Cu_yZn_{3-y}[Fe(CN)_6] + yZn^{2+} \quad (2)$$

$$KCu[Fe(CN)_6] + xM^{2+} \rightarrow KCu[M_xFe_{1-x}(CN)_6] + xFe^{2+}\ (M = Zn/Cu) \quad (3)$$

The morphological and compositional evolution of CuHCF is reported in Figure 4(c). In their study, CuHCF cubes and wires appeared after 500 cycles in comparison to the initial CuHCF nanoparticles morphology, and the Zn content within the cathode material was observed to increase upon cycling.[119] A detailed investigation of the Zn^{2+} insertion in the CuHCF structure was conducted by Renman and coworkers[64] by using operando synchrotron X-ray diffraction (XRD). They confirmed that the Zn^{2+} occupies both Fe $(CN)_6$ vacancy site (4a) and the cavity (8c) inside CuHCF cubic unit-cell, and a swapping of Zn^{2+} between the tunnels and the vacant Fe $(CN)_6$ sites was observed (Figure 4d). Even though the presence of a Zn-based new phase was not detected in the short term, it was proposed that the vacancies and their interaction with Zn^{2+} play a crucial role in the electrochemical performance of CuHCF/Zn system.

It is widely accepted Fe is the only active site in CuHCF, however some studies reported on the activity of both Cu and Fe in aqueous and organic electrolytes.[56,119,123–125] Gorlin et al.[122] presented an in-depth study of CuHCF cathode in AZIB cells by employing various X-ray spectroscopic techniques

(Figure 4e). It is suggested that the new phase formed during early charge/discharge cycles, can be attributed to the partial intercalation of $ZnSO_4$ into graphitic carbon. Combining XPS and XAS results, the electroactivity of Cu-site was confirmed. It is further concluded that Cu is the unstable species during aging, and the dissolution of Cu triggers Zn^{2+} ions to enter the Cu vacancies, instead of Fe vacancies, as well as the activation of Fe^{3+}/Fe^{2+} redox couple. On the intercalation mechanism of Zn^{2+} in CuHCF, the consensus is that a new second phase containing Zn ion is formed upon cycling. The composition, crystal structure, and the formation mechanism of the new second phase are still not fully elucidated, suggesting further research will be needed for a comprehensive understanding.

3.1.2. ZnHCF

Generally, hexacyanometallates present the typical PBAs structure with the involved transition metals being octahedrally coordinated with −CN- group, within a cubic unit cell (Fm-3 m). However, some ZnHCFs have been reported with an hexagonal configuration (R-3c), where the Zn^{2+} is tetrahedrally coordinated to the N atom of the −NC- ligand, as shown in Figure 5(a).[126–130] As reported by Rodriguez-Hernandez et al.,[126] the hexagonal (R-3c) cell, where both metal centers have saturated coordination with atoms from the framework, present a particularly high rigidity, leading to a more dense and robust
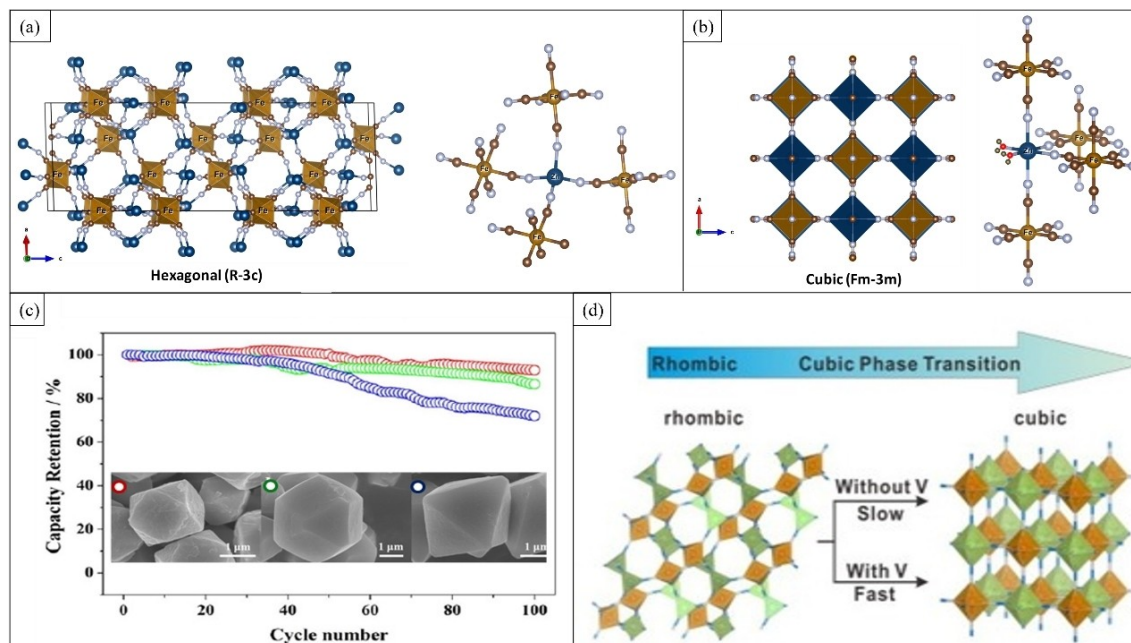
Batteries & Supercaps

Review
doi.org/10.1002/batt.202300340

**Chemistry
Europe**
European Chemical
Societies Publishing

Figure 5. a, b) Coordination environments of ZnHCF in rhombohedral phase and cubic phase. c) Cycle life test of shape-controlled RZnHCFs at 300 mA g^{-1}. Red, green, and blue circles represent C-RZnHCF, T-RZnHCF and O-RZnHCF, respectively. Reproduced with permission from Ref. [127]. Copyright (2015) The Author(s). d) Rhombic-Cubic ZnHCF phase transition in an aqueous environment. Reproduced with permission from Ref. [132]. Copyright (2016) Wiley-VCH Verlag GmbH & Co. KGaA, Weinheim.

structure. In a cubic structure, the coordination environment for the Zn atoms is normally formed by 4 N atoms from —NC-ligands and 2 H_2O molecules (Figure 5b). A structural transformation occurs when the coordinated water is removed by heating treatment. For example, a structure transformation from cubic phase to rhombohedral phase was observed during the dehydration process.[127,128] While Ng et al.,[129] Ding et al.[130] and Oliver-Tolentini et al.[131] found a monoclinic phase formed after heat treatment of a cubic (*fcc*) ZnHCF phase when heating between 75–220 °C.

The first ZIB cell, using ZnHCF in its rhombohedral phase as cathode material, and Zinc powder as the anode, was reported by Zhang et al.[67] The ZnHCF cathode exhibited an average operation voltage of 1.7 V in 1 M $ZnSO_4$, close to the discharge voltage of CuHCF. Because of its relatively high operation voltage, and a discharge capacity of 65.4 mAh g^{-1} (1 C) a specific energy density of 100 Wh kg^{-1} based on the total mass of the active electrode materials was achieved. The influence of morphology on the electrochemical performance of ZnHCF in 3 M $ZnSO_4$ electrolyte was also investigated. Polyhedral ZnHCF particles with cubooctahedral (C—RZnHCF), truncated octahedral (T—RZnHCF) and octahedral shape (O—RZnHCF), were synthesized. A structural transformation from cubic phase (as-prepared ZnHCF samples) to rhombohedral phase was observed by further dehydration at 70 °C. The study of the influence of shape and facets on the electrochemical performance showed that the ZnHCF sample with cubooctahedral morphology exhibited the best rate capability and cyclic stability, demonstrating a reversible Zn-ion intercalation mechanism, as shown in Figure 5(c). Thus, it has been concluded that the diffusion of zinc-ions and dissolution of active material is closely correlated with the structure of surface orientation.[127] ZnHCF undergoes rapid dissolution in Na_2SO_4 and K_2SO_4 aqueous electrolyte,[67] while it exhibits better structural stability in aqueous $ZnSO_4$ electrolytes. The observation has also been confirmed and reported by Ni et al.[132] They found that the capacity decay of ZIB cells in aqueous electrolytes is attributable to the loss of active materials (dissolution), which can be correlated with the structural changes observed upon cycling. A continuous change between rhombic (less soluble) and cubic (more soluble) structures takes place, accompanying the electrochemical redox reaction, as shown in Figure 5(d). By incorporating the Zn^{2+} ions in the electrolyte, the dissolution of cubic ZnHCF can be largely suppressed, and the capacity retention can be enhanced.

3.1.3. MnHCF

MnHCF has attracted much attention as promising cathode material for both Li-ion and post-Li ion batteries,[133] because of the abundancy and non-toxicity of the constituent elements, the large specific capacity derived from the two active redox couples, Fe^{3+}/Fe^{2+} and Mn^{3+}/Mn^{2+}, and the relatively high discharge voltage. Based on the different content of alkali metal, H_2O, and vacancies inside the structure, generally, AMnHCF (A: alkali metal ions) materials display three different structures, i.e., cubic, monoclinic, and rhombohedral (Figure 6a). For the monoclinic and the rhombohedral phase, the extraction/insertion of the cations in organic electrolytes is normally accompanied by the phase transformation from monoclinic/rhombohedral to cubic or tetrahedral.[34,134,135]
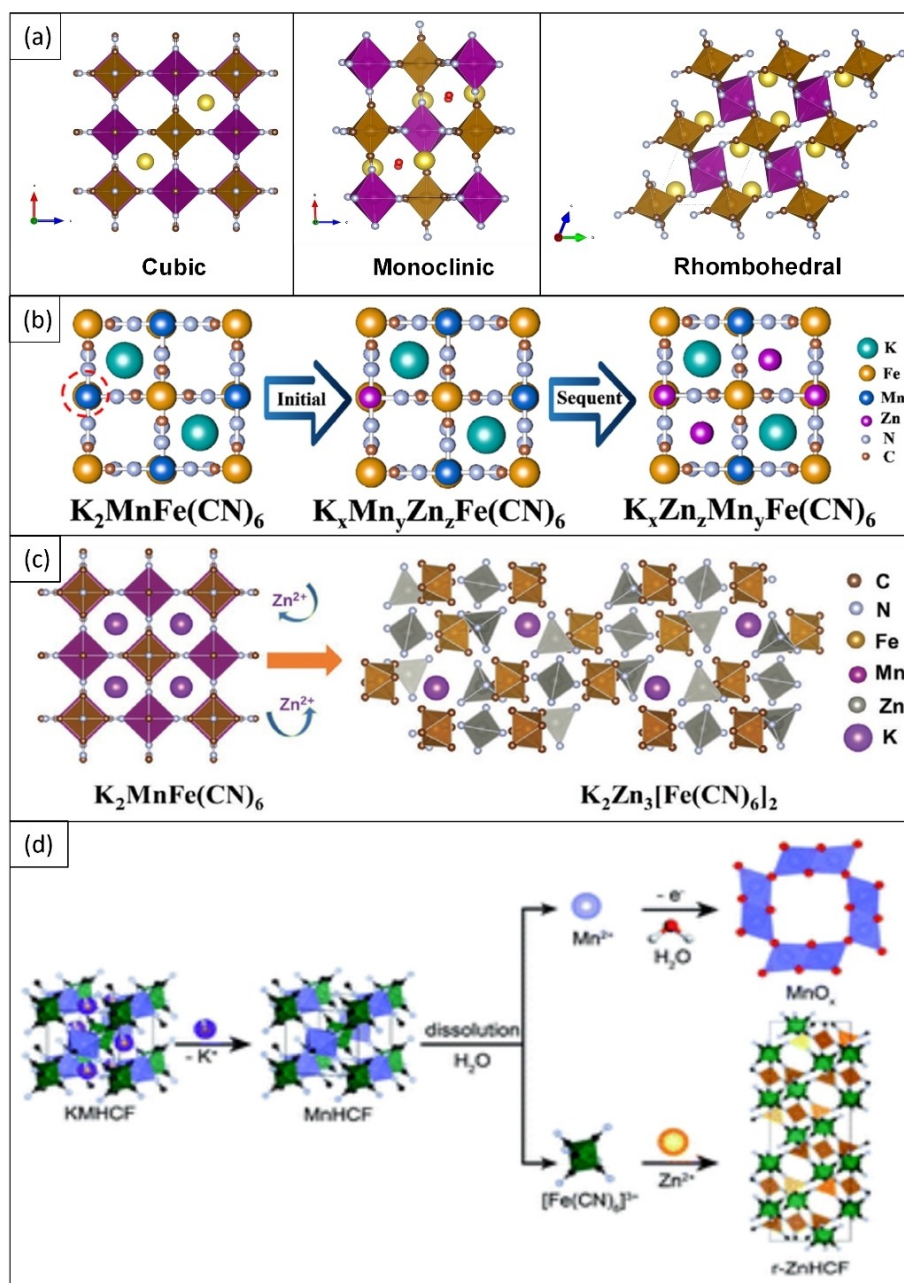
Figure 6. a) Cubic, Monoclinic and Rhombohedral phase structure of MnHCF. b) Schematic diagram of the insertion/extraction of Zn^{2+} in the KMHCF framework during the electrochemical process. Reproduced with permission from Ref. [93]. Copyright (2021) American Chemical Society. c) The schematic diagram of the phase transformation for KMnHCF electrode in 30 M KFSI + 1 M Zn $(CF_3SO_3)_2$ electrolyte. Reproduced with permission from Ref. [95]. Copyright (1999–2022) John Wiley & Sons, Inc. All rights reserved. d) The evolution of MnHCF in Zn^{2+} electrolyte. Reproduced with permission from Ref. [97]. Copyright (20022) The Royal Society of Chemistry.

On the other hand, the electrochemical performance of MnHCF in aqueous Zn-ion cells has displayed very different behavior. Indeed, while in organic electrolytes MnHCF is not soluble, in aqueous Zn-ion electrolyte, MnHCF suffers from severe dissolution, and a new phase containing Zn is formed upon cycling.[93,95–97] A high crystalline KMnHCF material, synthesized by Cao et al.[93] in the monoclinic phase, combined with metallic zinc anode, exhibited an excellent electrochemical performance providing a specific capacity of 140 mAh g^{-1} for the initial cycle at a current density of 100 mA g^{-1} (1 C) in 1 M

$ZnSO_4$ and 0.1 M $MnSO_4$ electrolyte. Interestingly, a phase transition of KMnHCF occurred during the first two cycles, and a new stable KZnMnHCF phase was formed, which presented the same crystal structure as $K_2Zn_3(Fe(CN)_6)_2$ (Figure 6b). Similar results were also reported by Deng et al.[95] (see Figure 6c), introducing a high voltage aqueous KMnHCF/Zn hybrid-ion cell using a 30 M KFSI/1 M Zn$(CF_3SO_3)_2$ electrolyte. The hybrid ZIB cell exhibited a maximum capacity of 138 mAh g^{-1} in the initial cycle, and the capacity stabilized at $\approx$ 100 mAh g^{-1} over 400 cycles at a current density of 0.2 A g^{-1}. Combining ab initio

Batteries & Supercaps

Review
doi.org/10.1002/batt.202300340

**Chemistry
Europe**
European Chemical
Societies Publishing

calculations and detailed characterizations, they underlined that the Zn^{2+} ion insertion not only induces an intense Jahn-Teller effect on the Mn^{3+}, but also replaces the framework Mn-sites and form a new KZnHCF phase. To trace and confirm where exactly Zn^{2+} resides within the structure during cycling, our group employed ex-situ XAS technique to record Mn, Fe and Zn k-edge spectra at different charge and discharge states. It was found that a −Zn−NC−Fe- structure was formed in all the cycled electrodes, which confirmed the partial replacement of Mn by Zn upon cycling, explaining the capacity decrease of MnHCF upon cycling due to the electrochemical inactivity of Zn.[96] To further understand the severe dissolution and the Zn displacement mechanism, Ni et al.[97] studied the effect of different Zn salts on the electrochemical performance of KMnHCF in 3 M $ZnSO_4$ and 3 M $Zn(OTf)_2$ electrolytes. It was observed that the electrochemical performance of the KMnHCF cathode was improved by changing the electrolyte from $ZnSO_4$ to $Zn(OTf)_2$. It was proposed that the $Zn(OTf)_2$ anion strongly absorbs on the electrode surface, thus preventing water oxidation and the decomposition of KMnHCF. The reported Zn ion intercalation mechanism included the KMnHCF transformation into the zinc hexacyanoferrate ($Zn_3[Fe(CN)_6]_2$) during the first charge process, coupled with the Mn ions' dissolution and re-deposition on the electrode as manganese oxides (Figure 6d) in the following discharge process. Even though the electrochemical test were conducted in different aqueous electrolytes, e.g., 1 M $ZnSO_4$ + 0.1 M $MnSO_4$,[93] 30 M KFSI + 1 M $Zn(CF_3SO_3)_2$[95] and 3 M $ZnSO_4$ or 3 M $Zn(CF_3SO_3)_2$,[97] the phase transformation from MnHCF to $Zn_3[Fe(CN)_6]_2$ rhombohedral phase were observed in all the reactions. The triggering mechanism and the evolution of this transformation in relation to the Fe-sites and Mn-sites are still not clearly understood and reported.

3.1.4. CoHCF/VHCF

Like $Fe^{2+/3+}$ and $Mn^{2+/3+}$ ions, cobalt ions also exhibit two possible oxidation states, i.e., Co^{2+} and Co^{3+} in the discharged and charged states respectively, and a facile electrochemical activity within the electrochemical stability window of the aqueous electrolyte. Ma et al.[102] proposed an aqueous rechargeable Zn-ion cell employing a cobalt hexacyanoferrate (CoHCF) cathode with a Zn anode providing a high capacity of 173.4 mAh g^{-1} at current density of 0.3 A g^{-1} and a high operational voltage of 1.75 V (vs. metallic Zn) in 4 M Zinc Trifluoromethanesulfonate ($Zn(OTf)_2$) hydrogel electrolyte. The structural evolution studies showed that the CoHCF framework and the overall morphology are well preserved during the Zn^{2+} insertion/extraction process, as shown in Figure 7(a), enabling a cycling stability for over 2200 cycles without any capacity decay with a coulombic efficiency approaching 100%. An all-solid-state Zn-ion battery cell was constructed by combing CoHCF cathode, metal Zn anode, and a solid polymer electrolyte of a poly (vinylidene fluoridehexafluoropropylene) film filled with poly (ethylene oxide)/ionic-liquid-based Zn salt. The all-solid-state Zn-ion cells showed excellent cycling performance of 30,000 cycles at 2 A g^{-1} at room temperature, withstanding high temperature up to 70 °C, and low temperature to −20 °C.[103]

Vanadium is another investigated transition metal, that exhibits several oxidation states, i.e., $V^{2+}/V^{3+}/V^{4+}/V^{5+}$. Vanadium based oxides, vanadate and vanadium phosphates have attracted widespread interest as promising electrode materials for AZIBs.[24,25,136–138] VHCF nanoparticles used as cathode material for an AZIBs, have been reported by Zhang et al.[105] The results showed that when cycled in 4 M $Zn(CF_3SO_3)_2$ electrolyte, VHCF exhibits two electrochemical redox active sites, V and Fe, responsible of three redox reactions at 0.71/0.51 V, 1.12/0.92 V
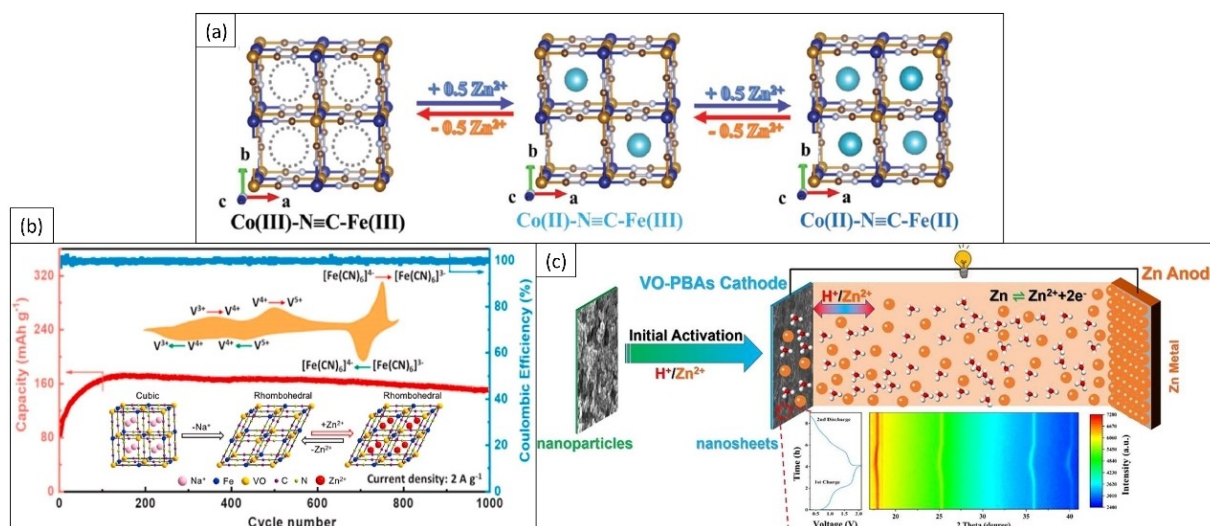

Figure 7. a) Schematic illustration of reversible Zn^{2+} intercalation/deintercalation in $CoFe(CN)_6$ frameworks during electrochemical process. Reproduced with permission from Ref. [102]. Copyright (2019) WILEY-VCH Verlag GmbH & Co. KGaA, Weinheim. b) Schematic illustration of the structural evolution of the VHCF during charge-discharge process, as well as the CV curve of VHCF electrode at 0.2 mV s^{-1}. Cycling performance and the corresponding Coulombic efficiency at a current density of 2 A g^{-1}. Reproduced with permission from Ref. [105]. Copyright (2020) Elsevier B.V. All rights reserved. c) Schematic illustration of the structural evolution of the VO-PBAs during charge-discharge process, as well as the electrochemical study of the VO-PBAs cathode in situ X-Ray diffraction. Reproduced with permission from Ref. [107]. Copyright (2021) Elsevier B.V. All rights reserved.

Batteries & Supercaps

Review
doi.org/10.1002/batt.202300340

Chemistry
Europe
European Chemical
Societies Publishing

and 1.85/1.71 V (vs Zn^{2+}/Zn), with a capacity of 187 mAh g^{-1} at current density of 0.5 A g^{-1}. During the first charging process, the cubic structure of VHCF changes to a rhombohedral phase, which further favors reversible Zn^{2+} ions insertion in subsequent cycles, as shown in Figure 7(b). Tian et al.[107] proposed a Zn/VO-PBAs aqueous system, by employing a "water-in-salt" electrolyte (21 M LiTFSI + 1 M ZnOTF). The as-fabricated cell achieved a high capacity of 209.6 mAh g^{-1} at 0.1 A g^{-1}, which is so far the highest capacity achieved for PBAs in AZIBs. It was reported that the VO-PBAs nanoparticles-based cathode converts to 2D nanosheets during the first several cycles, which promotes the fast electrolyte ions transport in the electrode materials (Figure 7c). Meanwhile, the co-insertion/extraction of the Zn^{2+}/H^+ during the electrochemical reaction contributes to the excellent electrochemical performance of the Zn/VO-PBA batteries. Based on the above results, we found CoHCF and VHCF electrodes exhibit much higher specific capacity than other PBAs electrodes. Although phase transformation was detected for CoHCF (cubic to monoclinic phase) and VHCF (cubic to rhombohedral phase), the framework substitution by Zn was not observed as instead reported forCuHCF and MnHCF electrodes.

3.2. Strategies to optimize the PBAs electrochemical performance in AZIBs

To improve the electrochemical stability and performance of PBAs cathode in aqueous Zn^{2+} electrolyte and mitigate or even suppress the dissolution of electrode material and reduce capacity fading, various optimization strategies for electrolytes, electrode materials and their interaction were proposed and adopted.

3.2.1. Electrolyte optimization

Although rechargeable aqueous batteries are attracting increasing attentions due to their low cost, high safety, environmentally friendly nature, and improved rate performance, the "free water" (the term "free water" indicates water molecules interacting solely with other water molecules)[139] molecules in aqueous electrolytes strongly limit the electrochemical stability window of the electrolyte and trigger multiple side reactions, thus affecting cell performance upon cycling. In order to suppress the activity of "free water" molecules and expand the electrochemical stability window, novel electrolytes and components have been proposed, including high concentrated electrolytes or "water-in-salt/gel" electrolytes,[78,82,87,95,97,105,107,140] hybrid electrolytes,[65,66,74,75,77,78,81–83,85,87,95,107,141,142] solid polymer electrolyte,[103] and additives,[84,86,88,89] to improve the electrochemical performances of AZIBs.

D. Kim et al.[140] reported that the cycling performance of ZnHCF in concentrated electrolyte (3 M $Zn(NO_3)_2$) was superior to that observed in the diluted system (1 M $Zn(NO_3)_2$), as a consequence of the decrease in the hydration number and radius of the zinc ions in the concentrated electrolyte. NiHCF

exhibits severe dissolution in diluted aqueous electrolyte (1 M $ZnSO_4$ or 1 M $Zn(TFSI)_2$), while a well-preserved NiHCF open framework was obtained in concentrated electrolyte (1 M $Zn(TFSI)_2 + 21$ M LiTFSI) or organic electrolyte (0.5 M $Zn(ClO_4)_2$ in acetonitrile), where the H_2O activity is highly suppressed by extensive coordination,[78] with similar results also reported by Deng et al.[95] (KMnHCF, 30 M KFSI + 1 M $Zn(CF_3SO_3)_2$), and Tian et al.[107] (VO-PBAs, 21 M LiTFSI + 1 M ZnOTF). Novel "water-in-gel" electrolytes were reported by Yang et al.[82] (FeHCF, 21 M LiTFSI + 1 M $Zn(TFSI)_2$-polyacrylamide gel electrolyte (HCZLE-PAM)), Pan et al.[66] (CuHCF-CNT, $NaCl/ZnSO_4$/Sodium alginate electrolyte) and Zhang et al.[69] (ZnHCF, $ZnSO_4$- carboxymethyl cellulose sodium (CMC)). A Zn│FeHCF cell with HCZLE-PAM (highly concentrated zinc and lithium trifluoromethanesulfony-limide electrolytes in the polyacrylamide) gel electrolyte exhibited 98% capacity retention with a Coulombic efficiency of $\approx 100\%$ after 100 cycles at 1 A g^{-1} when cycling at $-15\,°C$, highlighting the excellent anti-freezing function and the cycling stability of the cell.[82] Another report on a Zn│CuHCF-CNT cell, with $NaCl/ZnSO_4$/sodium alginate electrolyte, showed a high discharge voltage plateau of 2.1 V, large discharge specific capacity of 260 mAh g^{-1}, and a high capacity retention of 96.8% after 450 cycles.[66] The flexible coaxial-fiber aqueous ZnHCF rechargeable zinc-ion batteries (CARZIBs) fabricated by adopting Zn nanosheet arrays on carbon nanotube fiber as the core electrode and ZnHCF composite on aligned CNT sheets as outer electrode, with $ZnSO_4$/CMC gel electrolyte, delivered outstanding flexibility with a capacity retention of 93.2% after bending 3000 times.[69]

To further inhibit the activity of free water in aqueous electrolyte and extend the electrochemical window of aqueous electrolyte, Liu et al.[84] added 2 vol% vinylene carbonate (VC) to a 7 M $NaCF_3SO_3$/0.1 M $Zn(CF_3SO_3)_2$ aqueous electrolyte. It was observed that VC not only plays an important role in extending the electrochemical stability window, but also prevents the dissolution of the cathode material. Indeed, the aqueous FeHCF/Zn cell exhibited a good cycling stability with 60% capacity retention after 4000 cycles when cycled at 10 C. Xu et al.[86] proposed a hybrid aqueous electrolyte with mixed solvent of water and acetonitrile (ACN). Since ACN can form strong hydrogen-bonding interaction with water, an extension of the electrochemical windows was observed, as well as a decrease in side-reactions of the aqueous electrolyte. The aqueous FeHCF/Zn cell displayed extremely long cycle life with 51.4% capacity retention after 19000 cycles at 10 C in 1 M $NaCF_3SO_3$ (NaOTf) and 0.1 M Zn ($CF_3SO_3)_2$ H_2O/ACN electrolyte. A binary solvents system was also reported by Ni et al,[88] using triethyl phosphate (TEP) as co-solvent, in aqueous K/Zn electrolyte (0.5 M $Zn(CF_3SO_3)_2 + 1.5$ M KCF_3SO_3). The addition of TEP suppressed the water decomposition and increased the Coulombic efficiency. Hou et al.[89] developed an aqueous rechargeable hybrid battery by adding sodium dodecyl sulfate (SDS) in the Na_2SO_4 (1 M) and $ZnSO_4$ (1 M) electrolyte to increase the performance of $Na_2MnFe(CN)_6$ in aqueous Zn electrolyte and widen the electrochemical stability window. The SDS molecules can efficiently suppress the evolution of hydrogen and oxygen. The proposed $Na_2MnFe (CN)_6$/Zn cell delivered

Batteries & Supercaps

Review
doi.org/10.1002/batt.202300340

Chemistry
Europe
European Chemical
Societies Publishing

a specific capacity of 137 mAh g^{-1} with an operating voltage of about 2.0 V. Except using organic additives, generally, ZnHCF undergoes rapid dissolution in Na_2SO_4 and K_2SO_4 based electrolyte, while it is reported to be stable in aqueous $ZnSO_4$ electrolytes. Ni et al.[132] reported that the incorporation of Zn^{2+} ions in the electrolyte can largely suppress the dissolution of ZnHCF. Similarly, the KMnHCF material exhibits excellent electrochemical performance in 1 M $ZnSO_4$ and 0.1 M $MnSO_4$ electrolyte.[93]

3.2.2. Modification of electrode material

Synthesizing high-quality PBAs with low vacancy content and low crystal water content, especially coordinated water, is an efficient way to improve the electrochemical performances response of these compounds. As defined for PB, the low vacancy content means a transition from the "insoluble" structure of PBAs to "soluble" structure. Considering the structural design, particle size is another important influencing factor for realizing an excellent rate performance. Thus, multiple high-quality nanosized PBAs with particle size lower than 100 nm have been widely reported.[58,61,62,64–66,76–79,90,100,105,106]

Partial ion-substitution of PBAs, such as the reported Zn-substituted CuHCF,[63] Mn-substituted ZnHCF[73] and Co/Cu-substituted MnHCF,[90,92,98] is a promising way to suppress the dissolution and structure distortion of PBAs electrodes, and to increase the stability of PBAs cathodes for AZIBs. The CuZnHCF material reported by Kasiri et al.,[63] especially the sample with a Cu:Zn ratio of 93:7, exhibited an excellent cycle life up to 1000 cycles, with improved capacity retention with respect to the pure CuHCF counterpart. The Mn-substituted ZnHCF material introduced by Ni et al.,[73] revealed that the coexistence of Mn and Zn in the PBAs shows a synergistic effect on the electrochemical stability, resulting in superior cycle performance when compared to the PBAs with a single N-bonded metal (Mn or Zn). The sample with 7% Mn content exhibited the best cycle performance with 94% of the initial discharge capacity retained after 500 cycles at 250 mA g^{-1} (Figure 8a). In order to suppress the Jahn-teller distortion of Mn^{3+} and increase the specific capacity and cycling stability of MnHCF, Zeng et al.[92] synthesized Co-substituted Mn-rich PBA hollow sphere (CoMnP-BA HSs) as cathode material for AZIBs (see Figure 8c). The hollow structure not only provides a large surface area and sufficient active sites, but also accommodates the large volume change upon cycling. The as-prepared CoMnPBAs HSs electrode
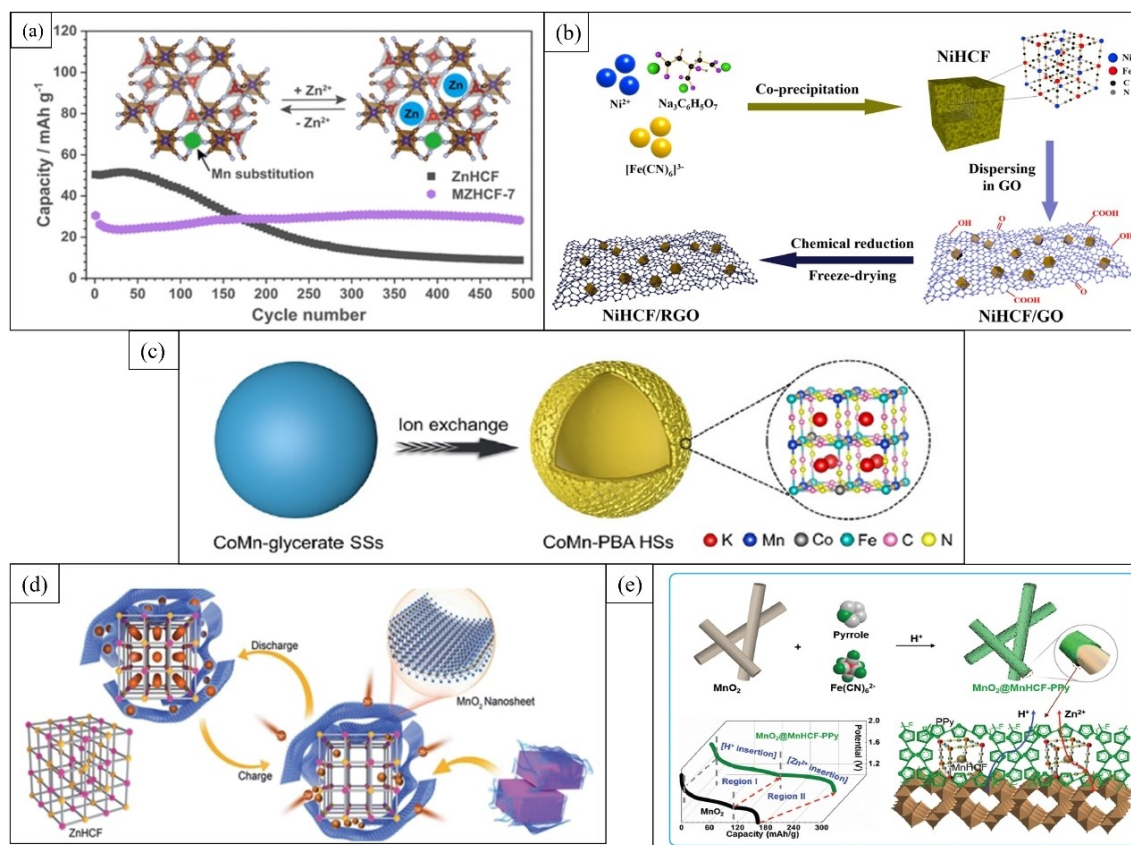

Figure 8. a) Galvanostatic charge/discharge of ZnHCF and MZHCF. Reproduced with permission from Ref. [73]. Copyright (2021) American Chemical Society. b) Schematic illustration of the synthetic process of NiHCF/RGO. Reproduced with permission from Ref. [79]. Copyright (2021) Elsevier Inc. All rights reserved. c) The synthetic process of CoMn-PBA HSs. Reproduced with permission from Ref. [92]. Copyright (2021) Wiley-VCH GmbH. d) Graphical illustration of the ZnHCF@MnO_2 electrode for Zn^{2+} storage. Reproduced with permission from Ref. [68]. Copyright (2017) The Royal Society of Chemistry. e) Schematic showing the in situ formed MnHCF-PPy composite interfacial layer that directs efficient H^+ and Zn^{2+} reversible (de)insertion into MnO_2 cathode. Reproduced with permission from Ref. [100]. Copyright (2022) The Royal Society of Chemistry.

Batteries & Supercaps

Review
doi.org/10.1002/batt.202300340

Chemistry Europe
European Chemical
Societies Publishing

exhibited high reversible capacity of 128.6 mAh g^{-1} at 0.05 A g^{-1}, good rate capability of 50 mAh g^{-1} at 2 A g^{-1}, as well as very promising cycling performance (76.4% capacity retention over 1000 cycles). Cu-substituted MnPBA double shelled nanoboxes (CuMnPBA DSNBs) were prepared by Zeng et al.,[98] highlighting that the partial Cu substitution and induced Mn vacancies inhibited the Jahn-Teller distortion, leading to superior cycling performance with a capacity retention of 96.8% after 2000 cycles.

To further extend the performance of PBAs, surface modification or coating with different carbon material (CNT, rGO),[79,143] conductive polymers (polyaniline (PANI), polypyrrole (ppy)[74,101] or other electroactive materials (MnO$_2$)[68,99,100] have been proposed to enable high conductivity, large capacity, and excellent cyclic stability. The NiHCF/RGO hybrid cathode material reported by Xue et al.[79] show that a strong synergy between NiHCF and highly conductive RGO effectively increases the specific surface area, accelerates the electron and ion transport, and inhibits the structural collapse of the NiHCF/RGO electrode during the Zn^{2+} insertion/extraction process (Figure 8b). A polyaniline (PANI) coating inhibits the dissolution of ZnHCF, enabling capacities as high as 150 mAh g^{-1}, and a capacity retention of 75% after 350 cycles.[74] A PPy coating increased the specific capacity and cycling stability of MnHCF in hybrid electrolyte of Li–Zn and K–Zn solution.[101] A MnO$_2$ wrapped zinc hexacyanoferrate (ZnHCF@MnO$_2$), combining the capacitive properties of MnO$_2$ and the interaction properties of ZnHCF, as shown in figure 8d, delivered a high capacity (118 mAh g^{-1} at 100 mA g^{-1}), good long-term stability and rate capability.[68] A bi-functional manganese hexacyanoferrate-poly-pyrrole (MnHCF–PPy) coating layer for MnO$_2$ was reported by Shang et al.,[100] combining the benefits of both PPy and MnHCF, where PPy films promoted the faster transformation of MnO$_2$ into MnOOH with the insertion of H$^+$, while MnHCF served as cation reservoirs to mediate continuous Zn ion transport, to keep lower the cation intercalation energy barrier, and to boost the Zn (de)insertion kinetics (Figure 8e). The MnO$_2$@MnHCF–PPy ZIB cell delivered a high discharge capacity (263 mAh g^{-1} at 0.5 C), remarkable rate capability (179 mAh g^{-1} at 5 C) and long lifespan in ZnSO$_4$ electrolyte.

3.2.3. Hybrid batteries

PBAs hybrid batteries, such as Li–Zn, Na–Zn, K–Zn, NH$_4^+$–Zn,[65,66,72,75,77,81,83,85,87,95,107,144,145] were proposed to combine the respective advantages of the two different chemistries to provide unique benefits (Figure 9). For instance, the Li$^+$–Zn^{2+}, Na$^+$–Zn^{2+}, K$^+$–Zn^{2+} and NH$_4^+$–Zn hybrid batteries can not only achieve high energy densities, but also support fast charging capabilities. As reported by Chunyang Li et al.,[65] the NH$_4^+$–Zn hybrid cell fabricated with CuHCF cathode, metallic Zinc anode, and mixed electrolyte (1 M (NH$_4$)$_2$SO$_4$+0.1 M ZnSO$_4$, pH~5.4) exhibited high working voltage (1.8 V), low self-discharge, and excellent rate capability. The Na–Zn CuHCF hybrid cell reported by Pan et al.[66] by using a novel "water-in-gel" electrolyte (NaCl/ZnSO$_4$/Sodium alginate electrolyte) achieved a high discharge voltage plateau of 2.1 V, and large discharge specific capacity of
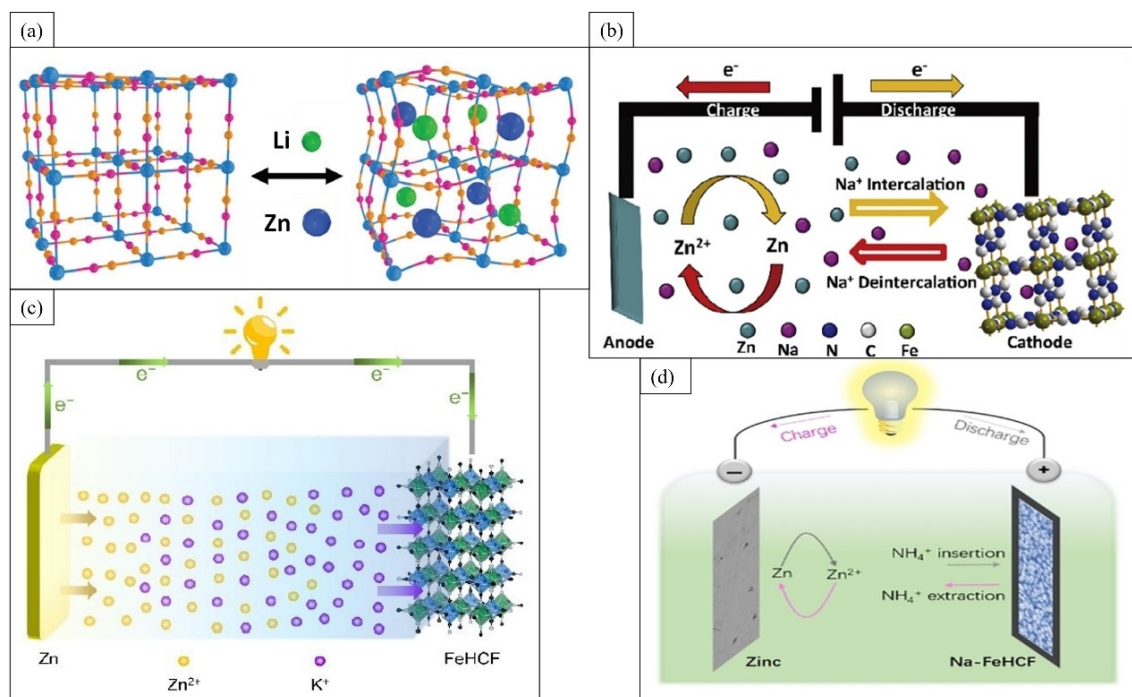

Figure 9. a) Schematic illustration of the FeHCF crystalline structure evolution under the (de−)insertion of Zn and Li ions. Reproduced with permission from Ref. [82]. Copyright (2019) WILEY-VCH Verlag GmbH & Co. KGaA, Weinheim. b) Schematic illustration of the redox reactions for NaFe–PB|Zn aqueous hybrid-ion cells. Reproduced with permission from Ref. [81]. Copyright (2017) Elsevier B.V. All rights reserved. c) Discharge scheme for the aqueous rechargeable FeHCF/K$^+$, Zn^{2+}/Zn hybrid cell. Reproduced with permission from Ref. [87]. Copyright (2021) Wiley-VCH GmbH. d) Schematic diagram of NaFeHCF|Zn NH$_4^+$–Zn hybrid battery cell. Reproduced with permission from Ref. [83]. Copyright (2019) Wiley-VCH Verlag GmbH & Co. KGaA, Weinheim.

Batteries & Supercaps

Review
doi.org/10.1002/batt.202300340

Chemistry
Europe
European Chemical
Societies Publishing

260 mAh g^{-1} with a superior energy density of 440 Wh kg^{-1}. The ZnHCF hybrid K–Zn system, proposed by Huang et al.,[72] exhibited a high discharge voltage of 1.937 V, and the cathode ZnHCF material displayed a capacity of 78.7 mAh g^{-1}, with 60% capacity retention at an extraordinarily high rate of 300 C. The Berlin Green (BG) K–Zn hybrid cell reported by Ni et al.,[87] in 3 mM Zn(OTf)$_2$ and 3 mM KOTf electrolyte, delivered high specific capacity of 169.2 mAh g^{-1} at 100 mA g^{-1}, excellent rate performance with 45.7 mAh g^{-1} at 6 A g^{-1}, and good long-term cyclability with a capacity retention of 57% over 1000 cycles at 1 A g^{-1}. It is proposed that the main intercalation cations in the hybrid battery is Na$^+$/K$^+$, due to their weak solvation effect and smaller electrostatic interaction, promoting the feasible surface reaction and rapid cation transportation, with Zn^{2+} ions staying at the surface rather than penetrating the bulk phase. With the right design and cathode material, hybrid cells can reach high energy density, long cycle life and improved charge-discharge rates. Combing the advantages of cost-effectiveness, safety and environmental friendliness, these hybrid batteries are particularly beneficial for applications where quick energy replenishment is required, such as high-power applications.

4. Summary and Outlook

In this review, we presented a comprehensive review of the structural modification and the reaction mechanisms occurring in several PBA materials for AZIBs with a particular focus on the Zn^{2+} intercalation mechanism and optimization strategies. As promising material for AZIBs, PBAs have gained significant attention. Indeed, AZIBs with PBAs as electrode material are generally considered safe and environmentally friendly. PBAs offer the potential for high energy density AZIBs, as well as the potential for large-scale production and implementation.

However, the application of PBAs in aqueous Zn-ion electrolytes still faces several challenges to be tackled. For instance, most PBAs suffer from severe dissolution and degradation upon cycling in aqueous Zn^{2+} electrolytes. To address these challenges, a comprehensive understanding of the Zn^{2+} intercalation mechanism in PBAs is crucial. In terms of redox activity, it is seen that both metal sites of PBAs are generally electroactive, even if to a different extent, and several electrochemical couples, such as Fe$^{3+/2+}$ and Mn$^{2+/3+}$, or Fe$^{3+/2+}$ and Cu$^{2+/+}$ have been reported. The studies on the Zn^{2+} intercalation process for CuHCF and MnHCF cathode materials have shown that a new Zn-based PBA or ZnHCF phase is formed during initial cycles, accompanied by the dissolution of Cu or Mn. However, the formation mechanism of the new ZnHCF phases in different Zn^{2+} electrolytes and its detailed composition, crystal structure, as well as the Cu or Mn dissolution mechanism and their existing states are still rather unexplored and discussed. So far, according to the studies reported, even though the electrochemical performance of CuHCF and MnHCF can be improved by optimizing the cathode material or electrolytes, the phase transformation cannot be fully suppressed. For this reason, more research efforts should be devoted to a comprehensive understanding of the underlying

mechanism of these compounds during cell operation (for instance by *operando* studies), particularly, focusing not only on the identification of the composition and phase (crystal structure) formed upon cycling, but also on the assessment of the metal electroactivity, for different PBAs in different aqueous Zn^{2+} electrolytes. For PB, the zinc insertion process is rarely reported. While the PB AZIBs can function not only as battery, but also as electrochromic devices. Thus, the study and development of PB AZIBs can extend the application of this bifunctional energy storable devices. For ZnHCF, CoHCF and VHCFA cathode material, although the pristine phases change from cubic to rhombohedral, or from cubic to monoclinic, the chemical composition of the framework is stable, with no Zn-substitution observed, especially for CoHCF and VHCF. Thus, the reason for the different intercalation process, as well as the factors that trigger the Zn substitution need further studies. Although the development and application of PBAs in AZIBs is still at an early stage, it is believed that a deep understanding of the mechanism of Zn^{2+} intercalation/release during the charge/discharge process can guide further developments of improved cathode materials and optimization strategies to mitigate or eliminate degradation, therefore ensuring extended cyclability and capacity retention.

Conflict of Interests

The authors declare no conflict of interest.

[1] F. Duffner, N. Kronemeyer, J. Tübke, J. Leker, M. Winter, R. Schmuch, *Nat. Energy* **2021**, *6*, 123–134.

[2] Y. Yu, Z. Guo, Y. Mo, Y. Lei, *EcoMat* **2020**, *2*, 2–4.

[3] Z. Pan, X. Liu, J. Yang, X. Li, Z. Liu, X. J. Loh, J. Wang, *Adv. Energy Mater.* **2021**, *11*, 1–24.

[4] G. Fang, J. Zhou, A. Pan, S. Liang, *ACS Energy Lett.* **2018**, *3*, 2480–2501.

[5] J. Liu, C. Xu, Z. Chen, S. Ni, Z. X. Shen, *Green Energy & Environ.* **2018**, *3*, 20–41.

[6] A. Konarov, N. Voronina, J. H. Jo, Z. Bakenov, Y. K. Sun, S. T. Myung, *ACS Energy Lett.* **2018**, *3*, 2620–2640.

[7] E. Grignon, A. M. Battaglia, T. B. Schon, D. S. Seferos, *iScience* **2022**, *25*, 104204.

[8] Y. Tian, Y. An, C. Wei, B. Xi, S. Xiong, J. Feng, Y. Qian, *Adv. Energy Mater.* **2021**, *11*, 1–33.

Batteries & Supercaps

Review

doi.org/10.1002/batt.202300340

Chemistry
Europe

European Chemical
Societies Publishing

[9] T. Yamamoto, T. Shoji, *Inorganic Chimica Acta* **1986**, *7*, 27–28.

[10] T. Shoji, M. Hishinuma, T. Yamamoto, *J. Appl. Electrochem.* **1988**, *18*, 521–526.

[11] B. Tang, L. Shan, S. Liang, J. Zhou, *Energy Environ. Sci.* **2019**, *12*, 3288–3304.

[12] Y. Shang, D. Kundu, *Curr. Opin. Electrochem.* **2022**, *33*, 100954.

[13] Y. Zou, T. Liu, Q. Du, Y. Li, H. Yi, X. Zhou, Z. Li, L. Gao, L. Zhang, X. Liang, *Nat. Commun.* **2021**, *12*, 1–11.

[14] J. Ma, M. Liu, Y. He, J. Zhang, *Angew. Chem.* **2021**, *133*, 12744–12755.

[15] W. Shang, Q. Li, F. Jiang, B. Huang, J. Song, S. Yun, X. Liu, H. Kimura, J. Liu, L. Kang, *Nano-Micro Lett.* **2022**, *14*, 1–13.

[16] M. H. Alfaruqi, V. Mathew, J. Gim, S. Kim, J. Song, J. P. Baboo, S. H. Choi, J. Kim, *Chem. Mater.* **2015**, *27*, 3609–3620.

[17] S. Islam, M. H. Alfaruqi, V. Mathew, J. Song, S. Kim, S. Kim, J. Jo, J. P. Baboo, D. T. Pham, D. Y. Putro, Y. K. Sun, J. Kim, *J. Mater. Chem. A* **2017**, *5*, 23299–23309.

[18] B. Lee, H. R. Lee, H. Kim, K. Y. Chung, B. W. Cho, S. H. Oh, *Chem. Commun.* **2015**, *51*, 9265–9268.

[19] B. Jiang, C. Xu, C. Wu, L. Dong, J. Li, F. Kang, *Electrochim. Acta* **2017**, *229*, 422–428.

[20] M. Song, H. Tan, D. Chao, H. J. Fan, *Adv. Funct. Mater.* **2018**, *28*, 1–27.

[21] J. Ming, J. Guo, C. Xia, W. Wang, H. N. Alshareef, *Mater. Sci. Eng. R* **2019**, *135*, 58–84.

[22] K. Zhu, T. Wu, K. Huang, *Energy Storage Mater.* **2021**, *38*, 473–481.

[23] W. G. Kidanu, J. Hur, H. W. Choi, M. Il Kim, I. T. Kim, *J. Power Sources* **2022**, *523*, 231060.

[24] Y. Liu, X. Wu, *J. Energy Chem.* **2021**, *56*, 223–237.

[25] L. Wang, K. W. Huang, J. Chen, J. Zheng, *Sci. Adv.* **2019**, *5*, 1–11.

[26] B. Xie, B. Sun, T. Gao, Y. Ma, G. Yin, P. Zuo, *Coord. Chem. Rev.* **2022**, *460*, 214478.

[27] J. Peng, W. Zhang, Q. Liu, J. Wang, S. Chou, H. Liu, S. Dou, *Adv. Mater.* **2022**, *2108384*, 1–20.

[28] A. Zhou, W. Cheng, W. Wang, Q. Zhao, J. Xie, W. Zhang, H. Gao, L. Xue, J. Li, *Adv. Energy Mater.* **2021**, *11*, 1–35.

[29] M. Ware, *J. Chem. Educ.* **2008**, *85*, DOI 10.1021/ed085p612.

[30] L. M. Cao, D. Lu, D. C. Zhong, T. B. Lu, *Coord. Chem. Rev.* **2020**, *407*, 213156.

[31] H. J. Buser, A. Ludi, D. Schwarzenbach, W. Petter, *Inorg. Chem.* **1977**, *16*, 2704–2710.

[32] M. Giorgetti, L. Guadagnini, D. Tonelli, M. Minicucci, G. Aquilanti, *Phys. Chem. Chem. Phys.* **2012**, *14*, 5527–5537.

[33] J. Agrisuelas, J. J. García-Jareño, D. Gimenez-Romero, F. Vicente, *J. Electrochem. Soc.* **2009**, *156*, P149.

[34] J. Song, L. Wang, Y. Lu, J. Liu, B. Guo, P. Xiao, J. J. Lee, X. Q. Yang, G. Henkelman, J. B. Goodenough, *J. Am. Chem. Soc.* **2015**, *137*, 2658–2664.

[35] A. Zhou, Z. Xu, H. Gao, L. Xue, J. Li, J. B. Goodenough, *Small* **2019**, *15*, 1–6.

[36] A. Mullaliu, G. Aquilanti, P. Conti, M. Giorgetti, S. Passerini, *ChemSusChem* **2020**, *13*, 608–615.

[37] J. Wu, J. Song, K. Dai, Z. Zhuo, L. A. Wray, G. Liu, Z. X. Shen, R. Zeng, Y. Lu, W. Yang, *J. Am. Chem. Soc.* **2017**, *139*, 18358–18364.

[38] F. M. Maddar, D. Walker, T. W. Chamberlain, J. Compton, A. S. Menon, M. Copley, I. Hasa, *J. Mater. Chem. A* **2023**, *11*, 15778–15791.

[39] I. June, V. D. Neff, *J. Electrochem.Soc.:Electrochemical Science and Technology* **1978**, *200*, 886–887.

[40] D. M. DeLongchamp, P. T. Hammond, *Adv. Funct. Mater.* **2004**, *14*, 224–232.

[41] O. Sato, *J. Solid State Electrochem.* **2007**, *11*, 773–779.

[42] B. Wang, M. Cui, Y. Gao, F. Jiang, W. Du, F. Gao, L. Kang, C. Zhi, H. Luo, *Solar RRL* **2020**, *4*, 2070036.

[43] C. X. Zhao, J. N. Liu, J. Wang, D. Ren, J. Yu, X. Chen, B. Q. Li, Q. Zhang, *Adv. Mater.* **2021**, *33*, 1–8.

[44] R. Koncki, *Crit. Rev. Anal. Chem.* **2002**, *32*, 79–96.

[45] R. Garjonyte, A. Malinauskas, *Biosens. Bioelectron.* **2000**, *15*, 445–451.

[46] C. D. Wessells, S. V. Peddada, R. A. Huggins, Y. Cui, *Nano Lett.* **2011**, *11*, 5421–5425.

[47] N. Kuperman, A. Cairns, G. Goncher, R. Solanki, *Electrochim. Acta* **2020**, *362*, 137077.

[48] Y. Luo, B. Shen, B. Guo, L. Hu, Q. Xu, R. Zhan, Y. Zhang, S. Bao, M. Xu, *J. Phys. Chem. Solids* **2018**, *122*, 31–35.

[49] N. Imanishi, T. Morikawa, J. Kondo, R. Yamane, Y. Takeda, O. Yamamoto, H. Sakaebe, M. Tabuchi, *J. Power Sources* **1999**, *81–82*, 530–534.

[50] Y. Tang, W. Li, P. Feng, M. Zhou, K. Wang, K. Jiang, *Chem. Eng. J.* **2020**, *396*, 125269.

[51] Y. Xu, S. Zheng, H. Tang, X. Guo, H. Xue, H. Pang, *Energy Storage Mater.* **2017**, *9*, 11–30.

[52] N. Imanishi, T. Morikawa, J. Kondo, Y. Takeda, O. Yamamoto, N. Kinugasa, T. Yamagishi, *J. Power Sources* **1999**, *79*, 215–219.

[53] A. Eftekhari, *J. Power Sources* **2004**, *126*, 221–228.

[54] C. D. Wessells, R. A. Huggins, Y. Cui, *Nat. Commun.* **2011**, *2*, 2–6.

[55] R. Y. Wang, B. Shyam, K. H. Stone, J. N. Weker, M. Pasta, H. W. Lee, M. F. Toney, Y. Cui, *Adv. Energy Mater.* **2015**, *5*, 1–10.

[56] Y. Mizuno, M. Okubo, E. Hosono, T. Kudo, K. Oh-Ishi, A. Okazawa, N. Kojima, R. Kurono, S. I. Nishimura, A. Yamada, *J. Mater. Chem. A* **2013**, *1*, 13055–13059.

[57] H. Park, Y. Lee, W. Ko, M. Choi, B. Ku, H. Ahn, J. Kim, J. Kang, J. K. Yoo, J. Kim, *Batteries & Supercaps* **2023**, *6*, e202200486.

[58] Z. Jia, B. Wang, Y. Wang, *Mater. Chem. Phys.* **2015**, *149*, 601–606.

[59] G. Zampardi, F. La Mantia, *Curr. Opin. Electrochem.* **2020**, *21*, 84–92.

[60] Y. Li, J. Zhao, Q. Hu, T. Hao, H. Cao, X. Huang, Y. Liu, Y. Zhang, D. Lin, Y. Tang, Y. Cai, *Mater. Today Energy* **2022**, *29*, 101095.

[61] R. Trócoli, F. La Mantia, *ChemSusChem* **2015**, *8*, 481–485.

[62] R. Trócoli, G. Kasiri, F. La Mantia, *J. Power Sources* **2018**, *400*, 167–171.

[63] G. Kasiri, J. Glenneberg, A. Bani Hashemi, R. Kun, F. La Mantia, *Energy Storage Mater.* **2019**, *19*, 360–369.

[64] V. Renman, D. O. Ojwang, M. Valvo, C. P. Gómez, T. Gustafsson, G. Svensson, *J. Power Sources* **2017**, *369*, 146–153.

[65] C. Li, J. Wu, F. Ma, Y. Chen, L. Fu, Y. Zhu, Y. Zhang, P. Wang, Y. Wu, W. Huang, *ACS Appl. Energ. Mater.* **2019**, *2*, 6984–6989.

[66] W. Pan, Y. Wang, X. Zhao, Y. Zhao, X. Liu, J. Xuan, H. Wang, D. Y. C. Leung, *Adv. Funct. Mater.* **2021**, *31*, DOI 10.1002/adfm.202008783.

[67] L. Zhang, L. Chen, X. Zhou, Z. Liu, *Adv. Energy Mater.* **2015**, *5*, 1–5.

[68] K. Lu, B. Song, Y. Zhang, H. Ma, J. Zhang, *J. Mater. Chem. A* **2017**, *5*, 23628–23633.

[69] Q. Zhang, C. Li, Q. Q. Li, Z. Pan, J. Sun, Z. Zhou, B. He, P. Man, L. Xie, L. Kang, X. Wang, J. Yang, T. Zhang, P. P. Shum, Q. Q. Li, Y. Yao, L. Wei, *Nano Lett.* **2019**, *19*, 4035–4042.

[70] M. S. Chae, S. T. Hong, *Batteries* **2019**, *5*, 1–13.

[71] Z. Chen, P. Wang, Z. Ji, H. Wang, J. Liu, J. Wang, M. Hu, Y. Huang, *Nano-Micro Lett.* **2020**, *12*, 1–12.

[72] M. Huang, J. Meng, Z. Huang, X. Wang, L. Mai, *J. Mater. Chem. A* **2020**, *8*, 6631–6637.

[73] G. Ni, X. Xu, Z. Hao, W. Wang, C. Li, Y. Yang, C. Zhou, L. Qin, W. Chen, X. Yao, J. Cai, *ACS Appl. Energ. Mater.* **2021**, *4*, 602–610.

[74] Q. Q. Liu, Z. Ma, Z. Chen, M. Cui, H. Lei, J. Wang, J. B. Fei, N. He, Y. Liu, Q. Q. Liu, W. Li, Y. Huang, *Chem. Commun.* **2022**, *58*, 8226–8229.

[75] K. Lu, B. Song, J. Zhang, H. Ma, *J. Power Sources* **2016**, *321*, 257–263.

[76] M. S. Chae, J. W. Heo, H. H. Kwak, H. Lee, S. T. Hong, *J. Power Sources* **2017**, *337*, 204–211.

[77] F. Ma, X. Yuan, T. Xu, S. Zhou, X. Xiong, Q. Zhou, N. Yu, J. Ye, Y. Wu, T. Van Ree, *Energy Fuels* **2020**, *34*, 13104–13110.

[78] Z. Li, T. Liu, R. Meng, L. Gao, Y. Zou, P. Peng, Y. Shao, X. Liang, *Energy Environ. Mater.* **2021**, *4*, 111–116.

[79] Y. Xue, Y. Chen, X. Shen, A. Zhong, Z. Ji, J. Cheng, L. Kong, A. Yuan, *J. Colloid Interface Sci.* **2022**, *609*, 297–306.

[80] Z. Liu, G. Pulletikurthi, F. Endres, *ACS Appl. Mater. Interfaces* **2016**, *8*, 12158–12164.

[81] L. P. Wang, P. F. Wang, T. S. Wang, Y. X. Yin, Y. G. Guo, C. R. Wang, *J. Power Sources* **2017**, *355*, 18–22.

[82] Q. Yang, F. Mo, Z. Liu, L. Ma, X. Li, D. Fang, S. Chen, S. Zhang, C. Zhi, *Adv. Mater.* **2019**, *31*, 0–17.

[83] C. Li, D. Zhang, F. Ma, T. Ma, J. Wang, Y. Chen, Y. Zhu, L. Fu, Y. Wu, W. Huang, *ChemSusChem* **2019**, *12*, 3732–3736.

[84] C. Liu, Y. Sun, J. Nie, D. Dong, J. Xie, X. Zhao, *New J. Chem.* **2020**, *44*, 4639–4646.

[85] X. Yuan, F. Ma, X. Chen, R. Sun, Y. Chen, L. Fu, Y. Zhu, L. Liu, F. Yu, J. Wang, Y. Wu, *Mater. Today Energy* **2021**, *20*, 100660.

[86] Z. Xu, B. Xiang, C. Liu, J. Sun, J. Xie, J. Tu, X. Xu, X. Zhao, *RSC Adv.* **2021**, *11*, 30383–30391.

[87] G. Ni, Z. Hao, G. Y. Zou, F. H. Cao, L. Qin, C. G. Zhou, *ChemElectroChem* **2022**, *9*, e202101351.

[88] G. Ni, M. Sun, Z. Hao, G. Zou, F. Cao, L. Qin, W. Chen, C. Zhou, *SSRN Electron. J.* **2022**, *31*, 101204.

[89] Z. Hou, X. Zhang, X. Li, Y. Zhu, J. Liang, Y. Qian, *J. Mater. Chem. A* **2017**, *5*, 730–738.

[90] N. Kuperman, M. Hopkins, S. Olson, G. Goncher, D. Evans, R. Solanki, *2018 IEEE 13th Nanotechnol. Mater. Devices Conf. NMDC 2018*, Portland, OR,USA, 10.1109/NMDC.2018.8605900.

[91] Q. Li, K. Ma, G. Yang, C. Wang, *Energy Storage Mater.* **2020**, *29*, 246–253.

[92] Y. Zeng, X. F. Lu, S. L. Zhang, D. Luan, S. Li, X. W. Lou, *Angew. Chem. Int. Ed.* **2021**, *60*, 22189–22194.

[93] T. Cao, F. Zhang, M. Chen, T. Shao, Z. Li, Q. Xu, D. Cheng, H. Liu, Y. Xia, *ACS Appl. Mater. Interfaces* **2021**, *13*, 26924–26935.

[94] W. Li, C. Xu, X. Zhang, M. Xia, Z. Yang, H. Yan, H. Yu, L. Zhang, W. Shu, J. Shu, *J. Electroanal. Chem.* **2021**, *881*, DOI 10.1016/j.jelechem.2020.114968.

[95] W. Deng, Z. Li, Y. Ye, Z. Zhou, Y. Li, M. Zhang, X. Yuan, J. Hu, W. Zhao, Z. Huang, C. Li, H. Chen, J. Zheng, R. Li, *Adv. Energy Mater.* **2021**, *11*, DOI 10.1002/aenm.202003639.

[96] M. Li, R. Sciacca, M. Maisuradze, G. Aquilanti, J. Plaisier, M. Berrettoni, M. Giorgetti, *Electrochim. Acta* **2021**, *400*, 139414.

[97] G. Ni, Z. Hao, G. Zou, X. Xu, B. Hu, F. Cao, C. Zhou, *Sustain. Energy Fuels* **2022**, *6*, 1353–1361.

[98] Y. Zeng, J. Xu, Y. Wang, S. Li, D. Luan, X. W. (David) Lou, *Angew. Chem.* **2022**, *321004*, DOI 10.1002/ange.202212031.

[99] J. Chen, L. Liao, B. Sun, X. Song, M. Wang, B. Guo, Z. Ma, B. Yu, X. Li, *J. Alloys Compd.* **2022**, *903*, DOI 10.1016/j.jallcom.2022.163833.

[100] Z. Shang, H. Zhang, M. Wang, Q. Chen, K. Lu, *Nanoscale* **2022**, *14*, 6085–6093.

[101] Y. Ruan, L. Chen, L. Cui, Q. An, *Coating* **2022**, 12, 779.

[102] L. Ma, S. Chen, C. Long, X. Li, Y. Zhao, Z. Liu, Z. Huang, B. Dong, J. A. Zapien, C. Zhi, *Adv. Energy Mater.* **2019**, *9*, 1–10.

[103] L. Ma, S. Chen, N. Li, Z. Liu, Z. Tang, J. A. Zapien, S. Chen, J. Fan, C. Zhi, *Adv. Mater.* **2020**, *32*, 1–10.

[104] C. Li, J. Li, X. Sun, H. Hou, J. Zhang, D. Zhang, J. Du, *Appl. Surf. Sci.* **2022**, *605*, DOI 10.1016/j.apsusc.2022.154660.

[105] Y. Zhang, Y. Wang, L. Lu, C. Sun, D. Y. W. Yu, *J. Power Sources* **2021**, *484*, 229263.

[106] S. Zhang, Q. Pang, Y. Ai, W. He, Y. Fu, M. Xing, Y. Tian, X. Luo, *Nanomaterials* **2022**, *12*, DOI 10.3390/nano12234268.

[107] Y. Tian, M. Ju, X. Bin, Y. Luo, W. Que, *Chem. Eng. J.* **2022**, *430*, 132864.

[108] Y. Xue, X. Shen, H. Zhou, J. Cao, J. Pu, Z. Ji, L. Kong, A. Yuan, *Chem. Eng. J.* **2022**, *448*, 137657.

[109] A. Dostal, B. Meyer, F. Scholz, U. Schröder, A. M. Bond, F. Marken, S. J. Shaw, *J. Phys. Chem.* **1995**, *99*, 2096–2103.

[110] N. F. Zakharchuk, N. Naumov, R. Stösser, U. Schröder, F. Scholz, H. Mehner, *J. Solid State Electrochem.* **1999**, *3*, 264–276.

[111] B. Lee, R. Seo, R. Lee, S. Yoon, H. Kim, K. Y. Chung, W. Cho, S. Hyoung, *ChemSusChem* **2016**, 9, 2948–2956.

[112] M. H. Alfaruqi, S. Islam, D. Y. Putro, V. Mathew, S. S. Kim, J. Jo, S. S. Kim, Y. K. Sun, K. Kim, J. Kim, *Electrochim. Acta* **2018**, *276*, 1–11.

[113] N. Becknell, P. P. Lopes, T. Hatsukade, X. Zhou, Y. Liu, B. Fisher, D. Y. Chung, M. G. Kanatzidis, N. M. Markovic, S. Tepavcevic, V. R. Stamenkovic, *Adv. Funct. Mater.* **2021**, *31*, 1–9.

[114] R. Zhang, P. Liang, H. Yang, H. Min, M. Niu, S. Jin, Y. Jiang, Z. Pan, J. Yan, X. Shen, J. Wang, *Chem. Eng. J.* **2022**, *433*, 133687.

[115] Z. Yang, X. Pan, Y. Shen, R. Chen, T. Li, L. Xu, L. Mai, *Small* **2022**, *18*, 1–8.

[116] W. Zhong, J. Zhang, Z. Li, Z. Shen, S. Zhang, X. Wang, Y. Lu, *Green Chem.* **2023**, DOI 10.1016/j.gce.2023.01.001.

[117] L. Kang, M. Cui, Z. Zhang, F. Jiang, *Batteries & Supercaps* **2020**, *3*, 966–1005.

[118] G. Kasiri, R. Trócoli, A. Bani Hashemi, F. La Mantia, *Electrochim. Acta* **2016**, *222*, 74–83.

[119] J. Lim, G. Kasiri, R. Sahu, K. Schweinar, K. Hengge, D. Raabe, F. La Mantia, C. Scheu, *Chem. Eur. J.* **2020**, *26*, 4917–4922.

[120] G. Kasiri, J. Glenneberg, R. Kun, G. Zampardi, F. La Mantia, *ChemElectroChem* **2020**, *7*, 3301–3310.

[121] G. Zampardi, M. Warnecke, M. Tribbia, J. Glenneberg, C. Santos, F. La Mantia, *Electrochem. Commun.* **2021**, *126*, DOI 10.1016/j.elecom.2021.107030.

[122] O. Dickson, S. Universitet, U. Universitet, M. Görlin, D. O. Ojwang, M. T. Lee, V. Renman, C. W. Tai, M. Valvo, *ACS Appl. Mater. Interfaces* **2021**, *13*, 59962–59974.

[123] O. Makowski, J. Stroka, P. J. Kulesza, M. A. Malik, Z. Galus, *J. Electroanal. Chem.* **2002**, *532*, 157–164.

[124] S. Yagi, M. Fukuda, T. Ichitsubo, K. Nitta, M. Mizumaki, E. Matsubara, *J. Electrochem. Soc.* **2015**, *162*, A2356–A2361.

[125] A. Mullaliu, G. Aquilanti, P. Conti, J. R. Plaisier, M. Fehse, L. Stievano, M. Giorgetti, *J. Phys. Chem. C* **2018**, *122*, 15868–15877.

[126] J. Rodríguez-Hernández, E. Reguera, E. Lima, J. Balmaseda, R. Martínez-García, H. Yee-Madeira, *J. Phys. Chem. Solids* **2007**, *68*, 1630–1642.

[127] L. Zhang, L. Chen, X. Zhou, Z. Liu, *Sci. Rep.* **2015**, *5*, 1–11.

[128] C. P. Krap, B. Zamora, L. Reguera, E. Reguera, *Microporous Mesoporous Mater.* **2009**, *120*, 414–420.

[129] C. W. Ng, J. Ding, L. M. Gan, *J.Phys.D: Appl. Phys.* **2001**, 34, *1188*.

[130] J. Ding, C. W. Ng, Y. Shi, *IEEE Trans. Magn.* **2001**, *37*, 2938–2940.

[131] M. Oliver-Tolentino, G. Ramos-Sánchez, G. Guzmán, M. Avila, I. González, E. Reguera, *Solid State Ionics* **2017**, *312*, 67–72.

[132] G. Ni, B. Han, Q. Li, Z. Ji, B. Huang, C. Zhou, *ChemElectroChem* **2016**, *3*, 798–804.

[133] M. Li, M. Gaboardi, A. Mullaliu, M. Maisuradze, X. Xue, G. Aquilanti, J. R. Plaisier, S. Passerini, M. Giorgetti, *ChemSusChem* **2023**, DOI 10.1002/cssc.202300201.

[134] H. Wang, E. Xu, S. Yu, D. Li, J. Quan, L. Xu, L. Wang, Y. Jiang, *ACS Appl. Mater. Interfaces* **2018**, *10*, 34222–34229.

[135] Y. Tang, W. Li, P. Feng, M. Zhou, K. Wang, Y. Wang, K. Zaghib, K. Jiang, *Adv. Funct. Mater.* **2020**, *30*, 1–9.

[136] G. Li, Z. Yang, Y. Jiang, C. Jin, W. Huang, X. Ding, Y. Huang, *Nano Energy* **2016**, *25*, 211–217.

[137] J. Zhou, L. Shan, Z. Wu, X. Guo, G. Fang, S. Liang, *Chem. Commun.* **2018**, *54*, 4457–4460.

[138] J. H. Lee, G. Ali, D. H. Kim, K. Y. Chung, *Adv. Energy Mater.* **2017**, *7*, DOI 10.1002/aenm.201601491.

[139] J. Han, A. Mariani, H. Zhang, M. Zarrabeitia, X. Gao, D. V. Carvalho, A. Varzi, S. Passerini, *Energy Storage Mater.* **2020**, *30*, 196–205.

[140] D. Kim, C. Lee, S. Jeong, *Iop. Conf. Ser. Mater. Sci. Eng.* **2018**, *284*, DOI 10.1088/1757-899X/284/1/012001.

[141] Z. Shen, S. Guo, C. Liu, Y. Sun, Z. Chen, J. Tu, S. Liu, J. Cheng, J. Xie, G. Cao, X. Zhao, *ACS Sustainable Chem. Eng.* **2018**, *6*, 16121–16129.

[142] Z. Liu, P. Bertram, F. Endres, *J. Solid State Electrochem.* **2017**, *21*, 2021–2027.

[143] M. N. T. Silva, J. D. Ardisson, J. D. Fabrisa, E. Nossol, *J. Braz. Chem. Soc.* **2020**, *31*, 1787–1795.

[144] Y. Hu, Y. Ye, B. Luo, H. Hu, X. Zhu, S. Wang, L. Li, S. Peng, L. Wang, *Adv. Mater.* **2018**, *30*, 1–6.

[145] T. Gupta, A. Kim, S. Phadke, S. Biswas, T. Luong, B. J. Hertzberg, M. Chamoun, K. Evans-Lutterodt, D. A. Steingart, *J. Power Sources* **2016**, *305*, 22–29.